Available online at www.sciencedirect.com
ScienceDirect
Journal of Sound and Vibration 309 (2008) 349–374
JOURNAL OF SOUND AND VIBRATION
www.elsevier.com/locate/jsvi

Dynamic analysis of slip damping in clamped layered beams with non-uniform pressure distribution at the interface

O. Damisa[a], V.O.S. Olunloyo[b,*], C.A. Osheku[a], A.A. Oyediran[c]

[a]*Department of Mechanical Engineering, Faculty of Engineering, University of Lagos, Lagos, Nigeria*
[b]*Department of Systems Engineering, Faculty of Engineering, University of Lagos, Lagos, Nigeria*
[c]*AYT Research Corp., McLean, VA 22102, USA*

Received 1 February 2006; received in revised form 26 January 2007; accepted 26 March 2007
Available online 25 October 2007

Abstract

Slip damping is a mechanism exploited for dissipating noise and vibration energy in aerodynamic and machine structures. Such slip in layered structures can be simulated by applying pressure to hold the members together at the interface. However, while most analyses of the mechanism assume an environment of uniform pressure at the interface, experiments to date have confirmed that this is rarely the case. There have been recent attempts to relax the restriction of uniform interface pressure to allow for more realistic pressure profiles that are encountered in practice. However, such works have mostly been limited to static loading for which it has been established that the interfacial pressure gradient does play a dominant role in modulating the level of energy dissipation. This paper is an attempt to extend such analyses to account for cases of realistic dynamic loading that drive such structural vibration in the first instance. In particular, it is shown that under dynamic loads, frequency variation more than non-uniformity in the interface pressure can have significant effect on both the energy dissipation and the logarithmic damping decrement associated with the mechanism of slip damping in such layered structures.

1. Introduction

Following the requirements of modern technology, there is increasing demand for machine tools with high stiffness, high damping capacity and light weight. Such requirements necessitated and popularised the use of welded and bolted layered cantilever beams as structural members. In the alternative cast layered cantilever beams can be used, but unfortunately, these are more expensive to produce. As a result, the deployment of welded and bolted layered beams is becoming increasingly common in the machine tool industry. Thus illustrations abound of links of the cantibeam model with real mechanical systems; one common case of practical significance is where a portion of a machine frame containing beam members is subjected to the action of bending load where the beam is fastened to a vertical or horizontal member at one end via bolted connections. Another example is in the line of industrial design of power plants, where the mounting of a gas

*Corresponding author. Tel.: +234 803 455 0838, +234 802 322 8015; fax: +234 1 5820841.
E-mail address: vosolunloyo@hotmail.com (V.O.S. Olunloyo).

0022-460X/$ - see front matter © 2007 Elsevier Ltd. All rights reserved.
doi:10.1016/j.jsv.2007.03.066

Nomenclature

b	width of laminated beam
$\frac{d}{dx}$	differential operator
E	modulus of rigidity
F	applied end force amplitude
h	depth of laminated beam
I	moment of inertia
L	length of laminated beam
P	clamping pressure at the interface of the laminated beams
t	time coordinate
u_1	displacement of the lower laminate
u_2	displacement of the upper laminate
W	dynamic response
W^F	transverse response in Fourier plane
x	space coordinate along the beam interface
z	space coordinate perpendicular to the beam interface

Greek letters

μ	coefficient of friction at the interface of the laminated beams
ξ	dummy variable
ρ	density of laminate material
$(\sigma_x)_1$	bending stress at the upper half of the laminates
$(\sigma_x)_2$	bending stress at the lower half of the laminates
τ_{xz}	shear stress at the interface of the laminated beams

turbine blade root in the holder (hub), can be well posed as a satisfactory idealisation of clamped sandwich elastic beams under harmonic excitation or bending load. In fact, this was one of the earliest contexts in which the problem was examined in the literature by Goodman and Klumpp [1].

Service failures of gas turbine blades can, in many cases, be attributed to high stresses accompanying resonant vibration. Such stresses are known to reduce not only the fatigue life of the blades in gas turbines but can cause damage even in cases of machine tool structures and equipment. This is particularly important for cases where in the construction of such machines, many of the components are fabricated in sections as built up beams or plates that are held together by bolted joints.

Consequently, the mechanism of damping as a means of controlling undesirable effects of vibration has received considerable attention in the literature over the years either in the context of aerodynamic structures or within the machine tool industry. There are in fact, several ways of effecting such damping; including the introduction of either constrained, unconstrained and even viscoelastic layers. One of such techniques is layered construction made possible by externally applied pressure that holds the members together at the interface. Under such circumstances, the profile of the interface pressure assumes a significant role, especially in the presence of slip, to dissipate the vibration energy. Another way of getting rid of unwanted vibration is through material damping as characterised by the strain energy of the structural member.

Within the context of the cantilever beam, one of the earliest works on slip damping is attributed to Goodman and Klumpp and although they are credited as the originators of the theory of slip damping, the topic has continued to attract the attention of researchers over the years. In fact, previous investigators such as Cockerham and Symmons [2], Hess et al. [3] and Gyran et al. [4] considered various friction and excitation models, while Barnett et al. [5] and Maugin et al. [6] considered interfacial or slip waves between two surfaces. The effect of viscoelasticity was also investigated by Gosz et al. [7] in the context of fiber-reinforced composites.

The nature of the interface pressure profile across the beam layer is a separate and important issue that has also received some attention over the years. Indeed, there are several ways of simulating such interfacial pressure including mechanisms such as bonded (welded) connections or the use of bolted connections and even bonded–bolted connections placed at appropriate locations along the laminate interface. Notwithstanding the importance of this issue, almost all previous analytical works have assumed a uniform pressure profile across the interface. However several workers, especially in the machine tool literature have tried to measure the actual nature of the pressure that is generated by investigating various forms of securing the layers.

Following the work of Goodman and Klumpp, early workers, such as Masuko et al. [8], Nishiwaki et al. [9,10], Motosh [11] had assumed uniform or constant intensity of pressure distribution at the interface of such

layered structures without considering the effects of surface irregularities and asperities. In metal-forming process of elastic beam structures, for example, surface irregularities appear in the form of microscopic structural composition defects arising from varying dislocation density especially in the region of plastic deformation. When such elastic structures are fastened via bolted connections, stress variation through the contacting layers occurs and tends to be maximum in the asperity junctions, which ultimately result in varying pressure distribution at the interface. Another property resulting from the handling of metals that can also affect the pressure distribution along such interface is the degree of alignment between the directions of lay on the surfaces of the two metal slices that define the laminate interface. In particular, when the direction of lay along the interface of different but adjoining slices of beam laminates are not properly aligned, such laminates do not make uniform contact when fastened together, resulting in variation in pressure distribution along the interface.

In fact, early studies from several authors such as Ferlund [12], Lardner [13], Sidorov [14], El-Zahry [15], Kaboyashi and Matsubayashi [16,17], Tsai and Chou [18], Shin et al. [19] and Song et al. [20] reported on the actual experimental values obtained for the pattern and intensity of pressure distribution at the interface of bolted joints and presented the corresponding damping characteristics for plates and shells.

In particular, Gould and Mikic [21]; Ziada and Abd [22] reported that the pressure distribution at the interface of a bolted joint is parabolic and has a circular influence zone circumscribing the bolt. The pressure profile was also reported to be independent of the tightening load applied.

Following the reported experimental results on the nature of the interfacial pressure distribution, recent workers have investigated the effect of non-uniformity in the pressure at the interface on the damping characteristics of such structures. Such analysis includes the work of Nanda and Behera [23,24].

On the analytical side, Hansen and Spice [25] have investigated the structural damping in laminated beams due to interfacial slip. In their formulation, a model in which slip can occur along the interface was analysed for a two-layered plate under the assumption that an adhesive layer of negligible thickness and mass, bonds the two adjoining surfaces such that a restoring force that is proportional to the amount of slip is created by the adhesive medium.

With the introduction of composite materials and the possible beneficial effects it can have on slip damping, several authors have revisited the problem of layered or jointed structures subjected to uniform pressure distribution. In this regard, Nanda [26] studied the effect of structural members under controlled dynamic slip while Nanda and Behera examined the problem of slip damping of jointed structures with connection bolts as found in machine structures [27]. Nanda and Behera [23,24,28] went further to studying the distribution pattern of the interface pressure as well as the damping capacity of such layered and jointed structures by carrying out both numerical analysis and experiments to ascertain the effects of a number of layers, diameter of bolts and use of washers.

One of the difficulties encountered in earlier analyses of this problem is the assumption of uniform pressure profile at the interface of the layers. Experiments and earlier analysis had clearly shown [12–15] that this was rarely the case. In fact, Gould and Mikic [21] and Ziada and Abd [22] established that the pressure distribution at the interface of bolted joints is parabolic in nature and its influence zone is roughly 3.5 times the diameter of the connecting bolt through which the restraining torque is applied. In particular, Nanda and Behera in their paper [27] were able to establish a polynomial expression for the resultant interface pressure emanating from such a bolt. However they went further than this by using Dunn's curve fitting software to calculate the exact spacing between bolts that would result in a uniform interfacial pressure distribution along the entire length of the beam. Using the exact spacing of 2.00211 times the diameter of the connecting bolts, Nanda and Behera were able to simulate an environment of uniform interface pressure and thereafter investigated the behaviour of dynamic slip damping.

The theoretical expression derived by Nanda and Behera in Ref. [27] for the pressure distribution at the interface of a bolted joint was obtained by curve fitting the earlier data reported by Ziada and Abd [22]. In particular, by postulating, a priori, an even function, they obtained an eighth-order polynomial in terms of the normalized radial distance from the centre of the bolt such that the function assumes its maximum value at the centre of the bolt and decreases monotonically radially. Their result also indicated that apart from the first two terms, the coefficients obtained for the polynomial were relatively insignificant. This suggests

that for a cantilever beam where interface pressure is effected through use of bolted joints, a linear profile radiating from the clamped end can be reasonably postulated as a first-order approximation for the pressure distribution across the interface. The argument here is not based on the pressure distribution profile around a single bolt but rather that if in actual practice a fairly uniform pressure can be achieved by carefully deploying a set of such bolts as was done by Nanda and Behera, further clamping of the built-in end of the cantilever that is usually used in experiments will superpose greater clamping pressure at the built-in end than at the free end, and such variation can, as in this case, be modelled as linear variation.

Furthermore, by following the method used by Nanda and Behera for simulating uniform interfacial pressure distribution, one mechanism for simulating a pressure gradient where the beams are held together by bolts, as in the case of Ziada and Abd, is to progressively vary monotonically (linearly for this case) the tightening torque on the securing bolts as one moves away from the clamped end to the free end of the cantilever beam. In any case, it is unlikely that the restraining torque on all the bolts can remain constant over time in actual practice.

The effect of non-uniform interface pressure distribution on the mechanism of slip damping for layered beams was also recently examined by Damisa et al. [29] but their analysis was limited to the case of static load. In particular, while the investigation by Damisa et al. [29] was limited to the case of linear pressure profile, the analysis in Olunloyo et al. [30] included other forms of interfacial pressure distributions such as polynomial or hyperbolic representations but the results obtained demonstrated that the effects of such distributions in comparison with the linear profile were largely incremental in nature and no fundamental differences were found. This provides additional justification for the linear pressure profile selected for the present investigation.

The aim of the present work is to extend our earlier analysis to cover the case of dynamic load so as to unravel the effect of the interplay between non-uniformity in interfacial pressure on the one hand as well as the frequency of the driving load on the other in the context of energy dissipation and logarithmic damping decrement.

2. Problem definition

As illustrated in Fig. 1, the problem here is to examine analytically the effect of the nature of load, frequency variation and the pressure gradient on

(i) the dynamic response of a clamped layered beam made from the same material and held together by some externally applied non-uniform force,
(ii) the profile of interfacial slip,
(iii) the slip energy dissipation under dynamic conditions, and
(iv) the logarithmic damping decrement associated with the mechanism of slip damping in such layered structures.

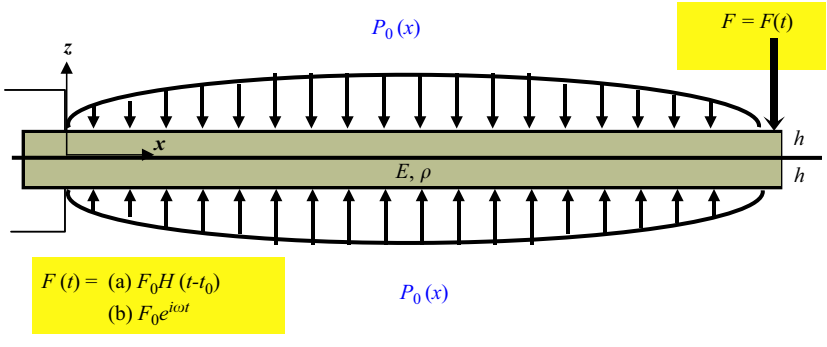

Fig. 1. Coordinate axes and geometry for layered beam from same material under dynamic load.

A general theory of the energy dissipation properties of press-fit joints in the presence of coulomb friction as originally developed by Goodman and Klumpp provides the basis for the physics of the problem. The contact conditions between the two layers are:

(i) there is continuity of stress distributions at the interface to sufficiently hold the two layers together both in the pre- and post-slip conditions,
(ii) a stick elastic slip with presence of coulomb friction occurs at the interface of the sandwich elastic beams to dissipate energy and does not remain constant as a function of some other variable such as spatial distance, time or velocity.

3. The dynamic response for linear interface pressure profile

For the case of layered beam of similar material, Osheku [31] has shown that the governing equation of motion can be written in the form:

$$\frac{\partial^4 W}{\partial x^4} + \beta \frac{\partial^2 W}{\partial t^2} = \alpha \frac{\mathrm{d}P(x)}{\mathrm{d}x}, \tag{1}$$

where the following parameters have been defined viz:

$$\alpha = \frac{6\mu}{Eh^2}, \quad \beta = \frac{\rho bh}{EI}.$$

We now introduce the Laplace transform namely:

$$\tilde{(\cdot)} = \int_0^\infty (\cdot) \mathrm{e}^{-st}\,\mathrm{d}t, \quad (\cdot) = \frac{1}{2\pi \mathrm{i}} \int_{\eta-\mathrm{i}\infty}^{\eta+\mathrm{i}\infty} \overline{(\cdot)} \mathrm{e}^{st}\,\mathrm{d}s. \tag{2}$$

When we take the Laplace transform of Eq. (1), we obtain:

$$\frac{\mathrm{d}^4 \tilde{W}(x,s)}{\mathrm{d}x^4} + \beta(s^2 \tilde{W}(x,s) - sW(0) - \dot{W}(0)) = \frac{\alpha}{s} \frac{\mathrm{d}P}{\mathrm{d}x}. \tag{3}$$

We limit our analysis for now to the case of linear pressure variation along the laminate interface namely:

$$P(x) = P_0\left(1 + \frac{\varepsilon}{L} x\right),$$

so that on substitution for the pressure in Eq. (3), we obtain

$$\frac{\mathrm{d}^4 \tilde{W}(x,s)}{\mathrm{d}x^4} + \beta(s^2 \tilde{W}(x,s) - sW(0) - \dot{W}(0)) = \frac{\alpha}{s} \frac{P_0 \varepsilon}{L}. \tag{4}$$

We next introduce the Fourier finite sine transform

$$\overline{[\cdot]} = \int_0^L [\cdot] \sin \frac{n\pi x}{L}\,\mathrm{d}x, \quad [\cdot] = \frac{2}{L} \sum_{n=1}^{\infty} \overline{[\cdot]} \sin \frac{n\pi x}{L}. \tag{5}$$

By invoking the following Fourier finite sine transform namely:

$$\begin{aligned} \Im_s(\tilde{W}_{xxxx}(x,s)) = {} & \frac{n^4\pi^4}{L^4} \tilde{W}^F(\lambda_n, s) - \frac{n^3\pi^3}{L^3}(\tilde{W}(0,s) + (-1)^{n+1} \tilde{W}(L,s)) \\ & + \frac{n\pi}{L}(\tilde{W}_{xx}(0,s) + (-1)^{n+1} \tilde{W}_{xx}(L,s)) \end{aligned} \tag{6}$$

and the boundary conditions at the clamped end of the beam in the Laplace transform plane as

$$\tilde{W}(0,s) = \frac{\mathrm{d}}{\mathrm{d}x} \tilde{W}(0,s) = \frac{\mathrm{d}^2}{\mathrm{d}x^2} \tilde{W}(L,s) = 0, \tag{7}$$

we may use the first and third conditions in the preceding equation to reduce Eq. (6) to

$$\Im_s(\tilde{W}_{xxxx}(x,s)) = \frac{n^4\pi^4}{L^4}\tilde{W}^F(\lambda_n,s) - \frac{n^3\pi^3}{L^3}(-1)^{n+1}\tilde{W}(L,s) + \frac{n\pi}{L}\tilde{W}_{xx}(0,s), \tag{8}$$

so that on assuming zero initial conditions for W, we obtain the Fourier sine transform of Eq. (3) as

$$\frac{n^4\pi^4}{L^4}\tilde{W}^F(\lambda_n,s) + \beta s^2\tilde{W}^F(\lambda_n,s) = \frac{\alpha}{s}\frac{P_0\varepsilon}{n\pi}(1+(-1)^{n+1}) + \frac{n^3\pi^3}{L^3}(-1)^{n+1}\tilde{W}(L,s) - \frac{n\pi}{L}\tilde{W}_{xx}(0,s). \tag{9}$$

To further simplify Eq. (9), we can proceed to evaluate the term $\tilde{W}_{xx}(0,s)$ by applying the Goodman and Klumpp end condition in the spatial-state form as

$$\int_0^h \tau_{(xz)_1}(x,t) = \frac{f(t)}{2b} \quad \text{at} \quad x = L. \tag{10}$$

By using the out-of-plane shear stress relation namely

$$\tau_{(xz)_1}(x,t) = \frac{1}{2}E(z^2 - hz)W_{xxx}(x,t) - \frac{\mu P}{h}(z-h), \tag{11}$$

we now rewrite Eq. (10) in the Laplace transform plane as

$$\int_0^L\int_0^h \frac{1}{2}E(z^2-hz)\tilde{W}_{xxx}(x,s)\,\mathrm{d}z\,\mathrm{d}x - \int_0^L\int_0^h \frac{\mu P}{h}(z-h)\,\mathrm{d}z\,\mathrm{d}x = \int_0^L \frac{\tilde{F}(s)}{2b}\,\mathrm{d}x. \tag{12}$$

Integration of this equation then reveals that the bending moment of the Euler–Bernoulli's clamped laminated beams admits the form:

$$\tilde{W}_{xx}(0,s) = \left(\frac{6\tilde{F}(s)}{Ebh^3} - \frac{1}{s}\frac{6\mu P_0}{Eh^2} - \frac{6\mu P_0\varepsilon}{sEh^2}\right)L. \tag{13}$$

This result clearly indicates that the value for expression (13) cannot be fully determined until the forcing function $f(t)$ is fully specified. Consequently, we limit our analysis to the following cases namely:

(a) $f(t) = F_0H(t-t_0)$,

where $H(t)$ is the Heaviside function and

(b) $f(t) = F_0\mathrm{e}^{\mathrm{i}\omega t}$.

4. Case of heaviside loading function

For this case, the forcing function is $f(t) = F_0H(t-t_0)$ and we evaluate the Laplace transform as $\tilde{F}(s) = (F_0/s)\mathrm{e}^{-t_0s} \equiv F_0\tilde{H}(s)$.

By recalling the only unutilised boundary condition in Eq. (7), viz $(\mathrm{d}/\mathrm{d}x)(\tilde{W}(0,s)) = 0$ and guided by the Laplace transform, we rewrite the bending moment as

$$\tilde{W}_{xx}(0,s) = \left\{\frac{6F_0\tilde{H}(s)}{Ebh^3} - \frac{1}{s}\frac{6\mu P_0}{Eh^2} - \frac{1}{s}\frac{6\mu P_0\varepsilon}{Eh^2}\right\}L. \tag{14}$$

Hence, the corresponding response of the Euler–Bernoulli's laminated beam in the Fourier–Laplace transform plane as presented in Eq. (9) admits the form:

$$\tilde{W}^F(\lambda_n,s) = \frac{\left(\frac{n^3\pi^3}{L^3}(-1)^{n+1}s\tilde{W}(L,s) - \frac{n\pi}{L}\left(\frac{6F_0}{Ebh^3} - \frac{6\mu P_0}{Eh^2} - \frac{6\mu P_0\varepsilon}{Eh^2}\right)L + \frac{\alpha P_0\varepsilon}{n\pi}(1+(-1)^{n+1})\right)}{\beta s(s-\mathrm{i}\omega_n)(v)}, \tag{15}$$

where $\omega_n^2 = n^4\pi^4/\beta L^4$ is the natural frequency of vibration of the clamped laminated beam as can be derived by setting the right-hand side of Eq. (9) to zero.

Our next step is to evaluate the Fourier inversion of Eq. (15) as

$$\tilde{W}(x,s) = \frac{\left(2s\tilde{W}(L,s)\sum_{n=1}^{\infty}(-1)^{n+1}\frac{\sin n\pi\bar{x}}{n\pi} + \frac{2L^3}{32}\alpha P_0\varepsilon\sum_{n=1}^{\infty}\frac{\sin 2n\pi\bar{x}}{n^5\pi^5} - 2L^3\left(\frac{6F_0}{Ebh} - \frac{6\mu P_0}{Eh^2} - \frac{6\mu P_0\varepsilon}{Eh^2}\right)\sum_{n=1}^{\infty}\frac{\sin n\pi\bar{x}}{n^3\pi^3}\right)}{\beta s(s-\mathrm{i}\omega_n)(s+\mathrm{i}\omega_n)\frac{L^4}{n^4\pi^4}}. \tag{16}$$

To further simplify the series in Eq. (16), we invoke the well-known closed-form Fourier series representations namely:

$$\bar{x} = \frac{1}{\pi}\sum_{n=1}^{\infty}\frac{(-1)^{n+1}}{n}\sin n\pi\bar{x}, \quad \forall\ 0<\bar{x}<1; \tag{17a}$$

$$\sum_{n=1}^{\infty}\frac{\sin n\bar{x}}{n^3} = \frac{\pi^2\bar{x}}{6} - \frac{\pi\bar{x}^2}{4} + \frac{\bar{x}^3}{12} \quad \forall\ 0<\bar{x}<2 \tag{17b}$$

and

$$\sum_{n=1}^{\infty}\frac{\sin n\bar{x}}{n^5} = \frac{\pi^4\bar{x}}{90} - \frac{\pi\bar{x}^3}{36} + \frac{\pi\bar{x}^4}{48} - \frac{\bar{x}^5}{240} \quad \forall\ 0<\bar{x}<2. \tag{17c}$$

Consequently, we can write Eq. (16) in the form:

$$\tilde{W}(\bar{x},s) = \left\{\left(\frac{2s\tilde{W}(L,s)\bar{x} - 2L^3\left(\frac{6F_0}{Ebh^3} - \frac{6\mu P_0}{Eh^2} - \frac{6\mu P_0\varepsilon}{Eh^2}\right)\left(\frac{\bar{x}}{6} - \frac{x^2}{4} + \frac{\bar{x}^3}{12}\right)}{\beta s(s-\mathrm{i}\omega_n)(s+\mathrm{i}\omega_n)\frac{L^4}{n^4\pi^4}}\right) + \left(\frac{L^3\frac{3\mu P_0\varepsilon}{8\,Eh^2}\left(\frac{\bar{x}}{45} - \frac{2\bar{x}^3}{9} + \frac{\bar{x}^4}{3} - \frac{2\bar{x}^5}{15}\right)}{\beta s(s-\mathrm{i}\omega_n)(s+\mathrm{i}\omega_n)\frac{L^4}{n^4\pi^4}}\right)\right\}. \tag{18}$$

By imposing the boundary condition $\partial\tilde{W}(0,s)/\partial\bar{x} = 0$ in Eq. (18), we can evaluate the deflection at the end of the laminated Euler–Bernoulli's cantilever beam in the Laplace domain as

$$\tilde{W}(L,s) = \left\{\frac{L^3}{s}\left(\frac{F_0}{Ebh^3} - \frac{\mu P_0}{Eh^2} - \frac{\mu P_0\varepsilon}{Eh^2}\right) - \frac{L^3}{s}\left(\frac{3}{(16)(45)}\frac{\mu P_0\varepsilon}{Eh^2}\right)\right\}. \tag{19}$$

Thus, we can now express Eq. (18) in the form:

$$\tilde{W}(\bar{x},s) = \frac{L^3\left(\left(\frac{F_0}{Ebh^3} - \frac{\mu P_0}{Eh^2}\right)(3\bar{x}^2 - \bar{x}^3) + \frac{\mu P_0\varepsilon}{Eh^2}\left(-3\bar{x}^2 + \frac{11\bar{x}^3}{12} + \frac{\bar{x}^4}{8} - \frac{\bar{x}^5}{20}\right)\right)}{\beta s(s-\mathrm{i}\omega_n)(s+\mathrm{i}\omega_n)\frac{L^4}{n^4\pi^4}}. \tag{20}$$

By invoking Laplace inversion

$$W(\bar{x},t) = \frac{1}{2\pi\mathrm{i}}\int_{\eta-\mathrm{i}\infty}^{\eta+\mathrm{i}\infty}\tilde{W}(\bar{x},s)\mathrm{e}^{s\hat{t}}\,\mathrm{d}s, \tag{21}$$

where

$$\hat{t} = t - t_0,$$

we find the dynamic response in state-space domain as

$$\bar{W}(\bar{x},\tau) = F_1(\tau)\left((1-\mu\bar{P}_0)(3\bar{x}^2 - \bar{x}^3) + \mu\bar{P}_0\varepsilon\left(-3\bar{x}^2 + \frac{11\bar{x}^3}{12} + \frac{\bar{x}^4}{8} - \frac{\bar{x}^5}{20}\right)\right) \tag{22}$$

and

$$F_1(\tau) = (1 - \cos 2\pi\tau),$$

where the following non-dimensionalised parameters have been introduced viz:

$$\bar{W}(\bar{x},\tau) = \frac{W(\bar{x},\tau)Ebh^3}{L^3F}, \quad \bar{P}_0 = \frac{P_0}{(F/bh)} \tag{23a}$$

and

$$\hat{t} = \frac{2\pi\tau}{\omega_n}. \tag{23b}$$

A casual examination of this result reveals that we can in fact extract the stationary solution as the earlier result reported for the case of static loading in Ref. [29] viz:

$$\bar{W}(\bar{x}) = \left((1-\mu\bar{P}_0)(3\bar{x}^2-\bar{x}^3) + \mu\bar{P}_0\varepsilon\left(-3\bar{x}^2 + \frac{11\bar{x}^3}{12} + \frac{\bar{x}^4}{8} - \frac{\bar{x}^5}{20}\right)\right).$$

4.1. Analysis of dynamic slip

As pointed out by Goodman and Klumpp [1], when microscopic slip occurs, there is relative displacement of points on opposite sides of the interface in the slipped region.

The dynamic relative slip at the interface of the laminated beam now reads:

$$\Delta u(x,t)_{z=0} = u_1(x,0^+,t) - u_2(x,0^-,t), \tag{24}$$

from which we rewrite relation (24) as

$$\Delta u(x,t)_{z=0} = E^{-1}\int_0^x \{(\sigma_x)_1(\xi,0^+,t) - (\sigma_x)_2(\xi,0^-,t)\}\,\mathrm{d}\xi, \tag{25}$$

where ξ is a dummy axial spatial variable of integration across the interface; 0^+, 0^- denote the origin of the transverse spatial variable for each layer and t is the time (state) variable.

We can in fact express the corresponding bending stress relations in state-space domain as

$$(\sigma_x)_1(x,z,t) = -\frac{E(2z-h)}{2}\frac{\partial^2 W(x,t)}{\partial x^2} + \frac{\mu P_{av}(x-L)}{h} \tag{26a}$$

and

$$(\sigma_x)_2(x,z,t) = -\frac{E(2z+h)}{2}\frac{\partial^2 W(x,t)}{\partial x^2} - \frac{\mu P_{av}(x-L)}{h}, \tag{26b}$$

so that Eq. (25) can be rewritten in the form:

$$\Delta u(\bar{x},\tau) = \int_0^{\bar{x}}\left\{h\frac{\partial^2\bar{W}(\bar{x},\tau)}{\partial\xi^2} + \frac{2\mu\bar{P}_{av}}{Eh}(\xi-1)\right\}\mathrm{d}\xi \tag{27}$$

and on introducing the non-dimensionalised parameters viz:

$$\Delta\bar{u} = \frac{\Delta u(\bar{x},\tau)Ebh^2}{L^2F}, \quad \bar{P}_{av} = \frac{P_{av}}{(F/bh)}.$$

Eq. (27) is integrated to give

$$\Delta\bar{u} = \frac{\partial\bar{W}}{\partial\bar{x}} + \mu\bar{P}_0(\bar{x}^2 - 2\bar{x}) + \mu\bar{P}_0\varepsilon\left(\frac{2}{3}\bar{x}^3 - \bar{x}^2\right), \tag{28}$$

where we have used the result

$$\bar{P}_{av} = \bar{P}_0\int_0^1 (1+\varepsilon\bar{x})\,\mathrm{d}\bar{x} = \bar{P}_0\left(1+\frac{\varepsilon}{2}\right),$$

so that substitution for $\bar{W}$ from Eq. (22) then gives the result

$$\Delta\bar{u} = \left\{ \begin{array}{l} [\mu\bar{P}_0(3F_1(\tau)+1) - 3F_1(\tau)](\bar{x}^2 - 2\bar{x}) \\ +\mu\bar{P}_0\varepsilon\left[-6F_1(\tau)\bar{x} + \left(\frac{11}{4}F_1(\tau) - 1\right)\bar{x}^2 + \left(\frac{F_1(\tau)}{2} + \frac{2}{3}\right)\bar{x}^3 - \frac{F_1}{4}(\tau)\bar{x}^4\right] \end{array} \right\}. \tag{29}$$

Furthermore, we can set $\varepsilon \to 0$ in Eq. (29) to obtain the dynamic slip at uniform pressure as

$$\Delta\bar{u} = (\mu\bar{P}_0(3F_1(\tau)+1) - 3F_1(\tau))(\bar{x}^2 - 2\bar{x}) \tag{30}$$

from which the parabolic profile $\Delta\bar{u} = (4\mu\bar{P}_0 - 3)(\bar{x}^2 - 2\bar{x})$ first derived by Goodman and Klumpp for the case of uniform interface pressure under static load can be recovered in the limit as $F_1(\tau) \to 1$ in Eq. (30).

4.2. Energy dissipation

The energy dissipated per cycle, following Goodman and Klumpp [1] is given by the relation

$$D = 4\mu b \int_0^{\pi/2\omega} \int_0^L P(x)\,\Delta u(x,t)\mathrm{d}x\,\mathrm{d}t, \tag{31}$$

which can also be expressed as

$$\bar{D} = 4\mu \int_0^{1/4} \int_0^1 \bar{P}_{av}\,\Delta\bar{u}\,\mathrm{d}\bar{x}\,\mathrm{d}\tau, \tag{32}$$

where $\bar{D} = D(\bar{x},\tau)Ebh^3/L^3F_0^2$ is the dimensionless dynamic energy dissipated so that on substituting for $\Delta\bar{u}$ from Eq. (29) we obtain

$$\bar{D} = \left[\left(\tfrac{8}{11}\mu\bar{P}_0 - \tfrac{46}{33}\mu^2\bar{P}_0^2\right) + \varepsilon\left(\tfrac{4}{11}\mu\bar{P}_0 - \tfrac{263}{165}\mu^2\bar{P}_0^2\right) - \tfrac{74}{165}\varepsilon^2\mu^2\bar{P}_0^2\right]. \tag{33}$$

Here again, by making appropriate substitutions in Eq. (33), the results for energy dissipation obtained by earlier workers who treated the static analysis of the problem can also be recovered.

5. Case of harmonic loading function

For this case, the forcing function is $f(t) = F_0 e^{i\omega t}$. This gives us the Laplace inversion as

$$\tilde{F}(s) = \frac{F_0}{s - i\omega}, \tag{34}$$

where ω is the excitation frequency.

By applying the technique used in Eqs. (16) and (17), we write that

$$\tilde{W}(\bar{x},s) = \frac{\left\{2s\tilde{W}(L,s)\bar{x} - 2L^3\left(\dfrac{6sF_0}{(s-i\omega)Ebh^3} - \dfrac{6\mu P_0}{Eh^2} - \dfrac{6\mu P_0\varepsilon}{Eh^2}\right)\Lambda_1 + \dfrac{3}{8}\dfrac{\mu P_0\varepsilon}{Eh^2}L^3\Lambda_2\right\}}{\beta s(s-i\omega_n)(s+i\omega_n)\dfrac{L^4}{n^4\pi^4}}, \tag{35}$$

where

$$\Lambda_1 = \left(\frac{\bar{x}}{6} - \frac{\bar{x}^2}{4} + \frac{\bar{x}^3}{12}\right), \quad \Lambda_2 = \left(\frac{\bar{x}}{45} - \frac{2\bar{x}^3}{9} + \frac{\bar{x}^4}{3} - \frac{2\bar{x}^5}{15}\right).$$

Use of the boundary condition $\partial\tilde{W}(0,s)/\partial\bar{x} = 0$ in Eq. (35) enables us to evaluate the deflection at the end of the laminated Euler–Bernoulli's cantilever beam in the Laplace domain as

$$\tilde{W}(L,s) = \left\{L^3\left(\frac{F_0}{(s-i\omega)Ebh^3} - \frac{\mu P_0}{sEh^2} - \frac{\mu P_0\varepsilon}{sEh^2} - \frac{1}{240s}\frac{\mu P_0\varepsilon}{Eh^2}\right)\right\}. \tag{36}$$

Subsequent substitution into Eq. (35) and carrying out the Laplace inversion for the non-dimensionalised variable as outlined in Eq. (23) gives the result

$$\bar{W}(\bar{x},t)=\left([F_2(t)-\mu\bar{P}_0F_1(t)](3\bar{x}^2-\bar{x}^3)+\mu\bar{P}_0F_1(t)\left(-3\bar{x}^2+\frac{11\bar{x}^3}{12}+\frac{\bar{x}^4}{8}-\frac{\bar{x}^5}{20}\right)\varepsilon\right), \tag{37}$$

where

$$F_1(t)=(1-\cos\,\omega_n t) \tag{38}$$

and

$$F_2(t)=\frac{1}{1-(\omega/\omega_n)^2}\left\{(\cos\,\omega t-\cos\,\omega_n t)+\mathrm{i}\left(\sin\,\omega t+\frac{\omega}{\omega_n}\sin\,\omega_n t\right)\right\}. \tag{39}$$

Here we have replaced the non-dimensionalisation introduced in Eq. (33a) with

$$\bar{W}=\frac{W(\bar{x},t)Ebh^3}{L^3F_0},\quad \bar{P}_0=\frac{P_0}{(F_0/bh)}. \tag{40}$$

We may also introduce the factor

$$\frac{\omega}{\omega_n}=\eta, \tag{41}$$

where η can be regarded as the associated frequency ratio.

If in addition we replace the non-dimensionalisation (23b) with

$$\frac{2\pi\tau}{\omega_n}=t, \tag{42}$$

this then allows us to rewrite our expressions for $F_1(t)$ and $F_2(t)$ as

$$F_1(t)=F_1(\tau)=(1-\cos\,2\pi\tau) \tag{43}$$

while

$$F_2(t)=F_2(\tau)=\frac{1}{(1-\eta^2)}\{(\cos(2\pi\eta\tau)-\cos 2\pi\tau)+\mathrm{i}(\sin(2\pi\eta\tau)+\eta\,\sin\,2\pi\tau)\}. \tag{44}$$

5.1. Evaluation of slip and energy dissipation

Following the procedure introduced for the case of Heaviside function, it is now possible to express the slip as

$$\Delta\bar{u}(\bar{x},\tau)=\left\{\begin{array}{l}[\mu\bar{P}_0(3F_1(\tau)+1)-3F_2(\tau)](\bar{x}^2-2\bar{x})\\ +\mu\bar{P}_0\varepsilon\left[-6F_1(\tau)\bar{x}+\left(\frac{11}{4}F_1(\tau)-1\right)\bar{x}^2+\left(\frac{1}{2}F_1(\tau)+\frac{2}{3}\right)\bar{x}^3-\frac{1}{4}F_1(\tau)\bar{x}^4\right]\end{array}\right\}. \tag{45}$$

Furthermore, the non-dimensionalised energy dissipated per cycle, for this case is given by

$$\bar{D}=\left\{\left(8\Delta(\eta)-\mu\bar{P}_0-\tfrac{46}{33}\mu^2\bar{P}_0^2\right)+\left(4\Delta(\eta)\mu\bar{P}_0\varepsilon-\tfrac{263}{165}\mu^2\bar{P}_0^2\varepsilon-\tfrac{74}{165}\mu^2\bar{P}_0^2\varepsilon^2\right)\right\}, \tag{46a}$$

where

$$\Delta(\eta)=\frac{1}{(1-\eta^2)}\left[\left(\frac{\sin\left((\pi/2)\,\eta\right)}{2\pi\eta}-\frac{1}{2\pi}\right)-\mathrm{i}\left(\frac{\cos\left((\pi/2)\eta\right)-1}{2\pi\eta}+\frac{\eta}{2\pi}\right)\right]. \tag{46b}$$

5.2. Analysis of logarithmic damping decrement

Logarithmic damping coefficient can be used as a measure of the damping capacity of a structure under consideration. In particular, we wish to examine to what extent the damping capacity is influenced by factors such as dynamic slip or interfacial pressure. Following Masuko et al. [8], the relationship between the energy dissipation from two consecutive cycles and the associated logarithmic damping decrement satisfies the relation

$$\delta = \frac{1}{2}\ln\left(\frac{E_n}{E_{n+1}}\right). \tag{47}$$

Here,

$$E_n = E_{ne} + E_{\text{loss}} \tag{48a}$$

and

$$E_{n+1} = E_n - E_{\text{loss}}, \tag{48b}$$

where E_{ne} is the strain energy of the laminate material, whereas E_{loss} is the energy loss per cycle and δ the logarithmic damping decrement.

By substituting for E_n, E_{n+1} from (48a) and (48b) respectively into Eq. (47), we obtain the relation

$$\delta = \tfrac{1}{2}\ln(1+\varphi_m), \tag{49}$$

where

$$\varphi_m = \frac{E_{\text{loss}}}{E_{ne}}.$$

In order to relate our work to the results of earlier workers such as Nanda and Behera [27] or Masuko et al. [8], we define the damping ratio Ψ as

$$\Psi = \frac{E_{\text{loss}}}{E_{ne}+E_{\text{loss}}} = \frac{\varphi_m}{1+\varphi_m}. \tag{50}$$

Thus,

$$\varphi_m = \frac{\Psi}{1-\Psi} \tag{51}$$

and

$$\delta = \frac{1}{2}\ln(1+\varphi_m) = \frac{1}{2}\ln\left(\frac{1}{1-\Psi}\right). \tag{52}$$

Hence, by computing either Ψ or φ_m we can evaluate δ.

However, in order to compute Ψ or φ_{m} we need to find E_{ne} and E_{loss}.

Our point of departure is that E_{loss} and E_{ne} are computed differently here than what was done by earlier workers. In particular, E_{loss}, the slip energy is computed from Eq. (46a), i.e., $\bar{D}$, whereas E_{ne} is presently analysed.

5.3. Analysis of strain energy of the clamped laminated beams

The total strain energy of the clamped laminated cantilever beams for our problem is a combination of the energy introduced by the bending moment as well as that stored from the deflection of the free end. The energy from the bending moment is given by the theorem of Castigliano as

$$U_1 = \int_0^L \frac{M^2}{2EI}\,\mathrm{d}x \tag{53}$$

while the energy stored at the free end is computed from the theory of strength of materials as

$$U_2 = \frac{3}{2}\frac{EI}{L^3} W_L^2. \tag{54}$$

Here, M is the bending moment; E the modulus of rigidity of the material; $I = 2/3bh^3$ is the moment of inertia of the clamped laminated beam and W_L the deflection at the free end.

For our problem, we calculate our non-dimensionalised strain energy components as

$$\bar{U}_1 = 27\{e^{i4\pi\eta} - 2\mu\bar{P}_0(1+\varepsilon)e^{i2\pi\eta} + \mu^2\bar{P}_0^2(1+2\varepsilon+\varepsilon^2)\} \tag{55}$$

and

$$\bar{U}_2 = \left\{e^{i4\pi\eta} - 2\mu\bar{P}_0\left(1+\frac{241\varepsilon}{240}\right)e^{i2\pi\eta} + \mu^2\bar{P}_0^2\left(1+\frac{241}{120}\,\varepsilon + \left(\frac{241}{240}\right)^2\varepsilon^2\right)\right\}, \tag{56}$$

where we have introduced the non-dimensionalisation

$$\bar{U}_n = \frac{U_n E b h^3}{F_0^2 L^3}, \quad n = 1, 2.$$

This now allows us to write

$$\delta = \frac{1}{2} Ln\left(1 + \frac{\bar{D}}{\bar{U}_1 + \bar{U}_2}\right). \tag{57}$$

To be sure, we note that the formula derived for computing δ as reported by Nanda and Behera [27] as well as in the theoretical analysis of Masuko et al. [8] was based on invoking the Maclaurin series in the asymptotic limit $\Psi \ll 1$ (i.e. $E_{\text{loss}} \ll E_{ne}$), whereas the present results as computed from Eqs. (42) and (47), do not suffer from such a restriction and should hold for a wider spectrum of Ψ. However, they should also converge to the results of Nanda and Behera, Masuko et al. and earlier workers as the frequency spectrum approaches regions where $E_{ne} \gg E_{\text{loss}}$ must necessarily hold.

An important point made by Nanda and Behera [27] relates to the dependence of the logarithmic damping decrement on the number of interfacial layers. In particular, an expression was derived which showed that if m laminates are jointed together with connecting bolts to construct multi-layered cantilever beams, the damping ratio of such beams increases with the number of laminates as this arrangement ensures that there would be some $m-1$ interfaces where slip and therefore damping can occur. For our problem, the issue is to predict what modifications are to be incorporated if the number of laminates exceeds two. The authors have in fact derived results for multi-layered similar and dissimilar sandwich elastic and viscoelastic beams, but the details of this will be published elsewhere.

6. Analysis of results

In discussing our results we would like to investigate to what extent the response, slip and dissipated energy are affected by the frequency of the forcing function. Damisa [32] for example has established that when the interfacial pressure is uniform the maximum energy that can be dissipated by slip can in fact exceed the value reported by Goodman and Klumpp for their problem. In coming to this conclusion, Damisa carried out a limit analysis in the neighbourhood of the resonance frequency.

More recently, other workers such as Damisa et al. [29] and Olunloyo et al. [30] have also shown that by carefully selecting the interfacial pressure profile, slip energy dissipation in excess of that reported by Goodman and Klumpp can be arranged for the case where the cantibeam is subjected to static external load. The interest here is to see if the maximum energy that can be arranged where the applied external load is a dynamic forcing function is also frequency dependent or if it is solely a function of the interfacial pressure profile.

Figs. 2 and 3 show the displacement and slip at the free end of the cantilever beam while Fig. 4 displays the dissipated energy for the entire structure at the indicated frequency factor $\eta = \sqrt{3}/2$.

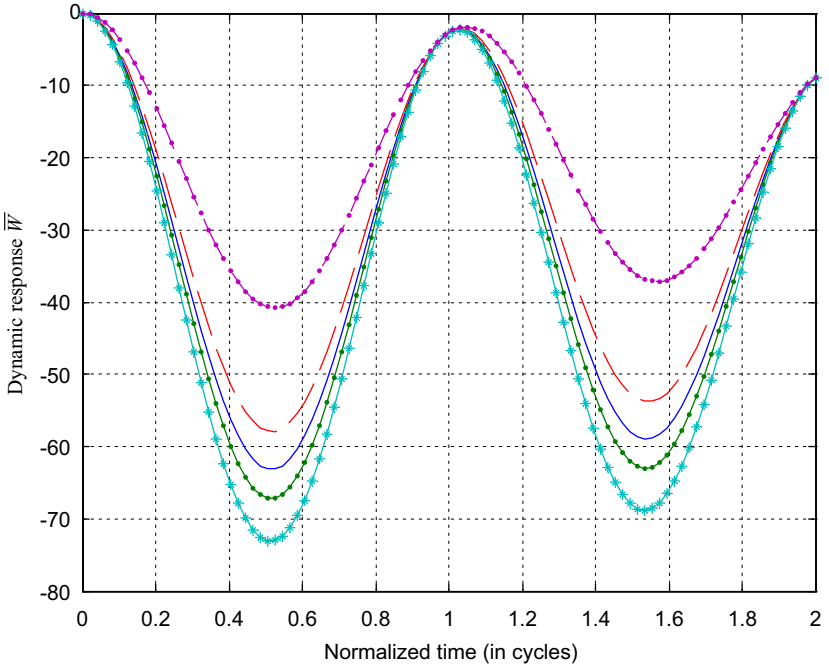

Fig. 2. Dynamic response profile at the free end of the cantibeam at optimum interfacial pressure for case $\eta = \sqrt{3}/2$. — $\varepsilon = 0$; $\varepsilon = 0.2$; ------ $\varepsilon = -0.2$; $\varepsilon = 0.6$; $\varepsilon = -0.6$.

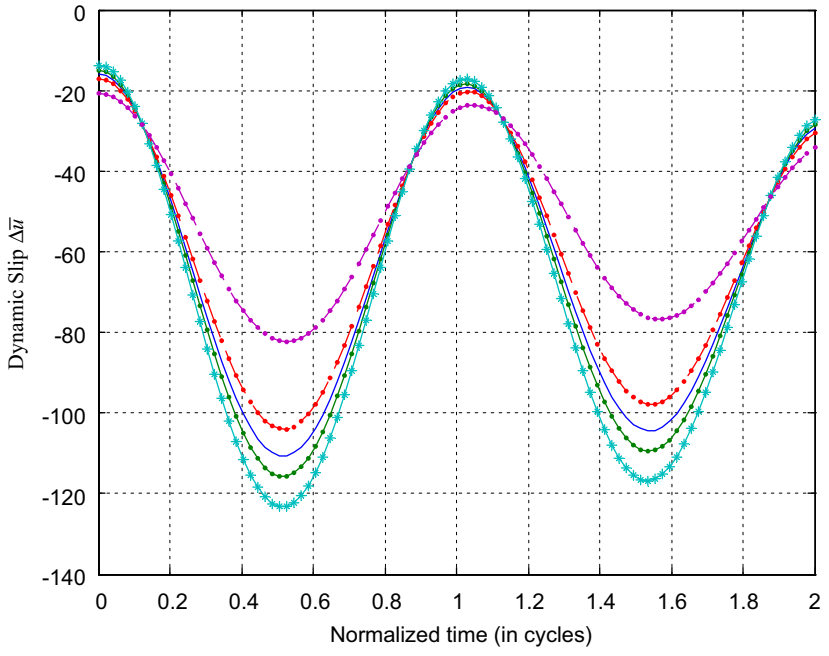

Fig. 3. Dynamic slip profile at the free end of the cantibeam at optimum interfacial pressure for case $\eta = \sqrt{3}/2$. — $\varepsilon = 0$; $\varepsilon = 0.2$; ------ $\varepsilon = -0.2$; $\varepsilon = 0.6$; $\varepsilon = -0.6$.

It is significant that irrespective of the value of the pressure gradient ε, the energy dissipation assumes the same parabolic profile reported for the static case by earlier workers. This is a direct consequence of the derived expression for energy dissipation viz: Eq. (46a), from which we can deduce that the condition for

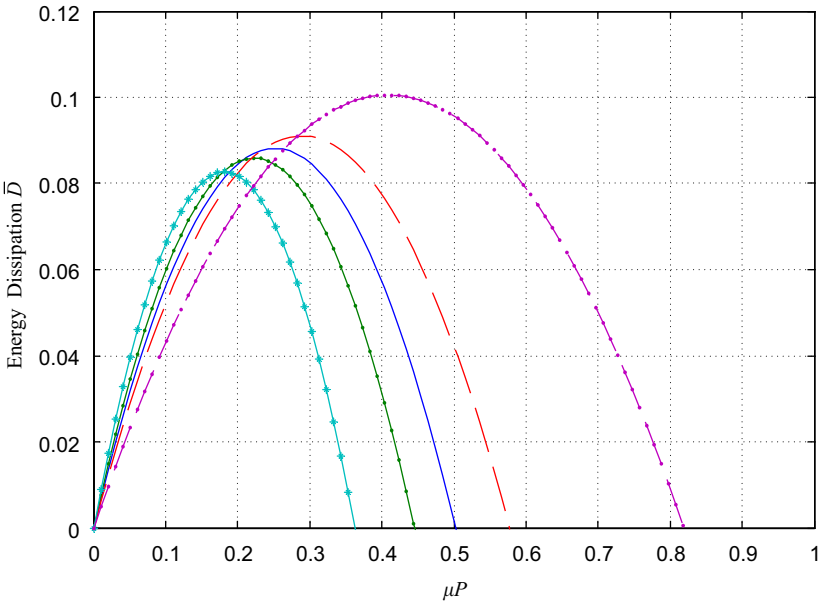

Fig. 4. Dynamic energy dissipation profile at $\eta = \sqrt{3}/2$. — $\varepsilon = 0$; —●— $\varepsilon = 0.2$; ------ $\varepsilon = -0.2$; —✳— $\varepsilon = 0.6$; —●— $\varepsilon = -0.6$.

optimal energy dissipation is given by

$$\mu P_{\text{opt}} = \frac{(2+\varepsilon)\,\Delta(\eta)}{\left(\frac{23}{33} + \frac{263}{330}\varepsilon + \frac{37}{165}\varepsilon^2\right)} = J\,\Delta(\eta), \tag{58a}$$

where

$$J = J(\varepsilon) = \frac{(2+\varepsilon)}{\left(\frac{23}{33} + \frac{263}{330}\varepsilon + \frac{37}{165}\varepsilon^2\right)}. \tag{58b}$$

This result highlights the effects of the pressure gradient ε on the one hand and the associated frequency ratio η, on the other. The relation (58a) also confirms that even in the absence of interfacial pressure gradient, the frequency of the load has a significant role to play in defining the optimal pressure for slip damping.

Also note that from relation (58a) it is now possible to compute the optimal energy dissipation from Eq. (46a) as

$$\bar{D}_{\text{opt}} = J\Delta^2\left\{\left(8 - \tfrac{46}{33}J\right) + \varepsilon\left(4 - \tfrac{263}{165}J\right) - \tfrac{74}{165}J\varepsilon^2\right\} \tag{59}$$

which clearly demonstrates that the optimal slip energy is modulated by the coefficient Δ^2 which derives from the frequency ratio η as earlier defined in relation (46b). In particular, we note that in the absence of pressure gradient (i.e. $\varepsilon = 0$) we obtain:

$$\bar{D}_{\text{opt}} = \tfrac{264}{23}\Delta^2 < \tfrac{3}{2} \quad \text{for } 0 < \eta < 1$$

as can be confirmed from the plot for Δ in Fig. 11. This means that the maximum energy that can be dissipated through dynamic slip is always less than what is obtained in the static case even for the case of uniform interfacial pressure. This agrees with the experimental results of Goodman and Klumpp.

In order to have a better appreciation of the interplay of parameters, typical results for the beam deflection and interfacial slip have also been displayed in three dimensions in Figs. 5(a,b) and 6(a,b), respectively. It is however to be noted that the graphs for the case of uniform interfacial pressure, i.e. $\varepsilon = 0$ as plotted in Figs. 2 and 3 appear similar to the oscilloscope photographs reported by Goodman and Klumpp.

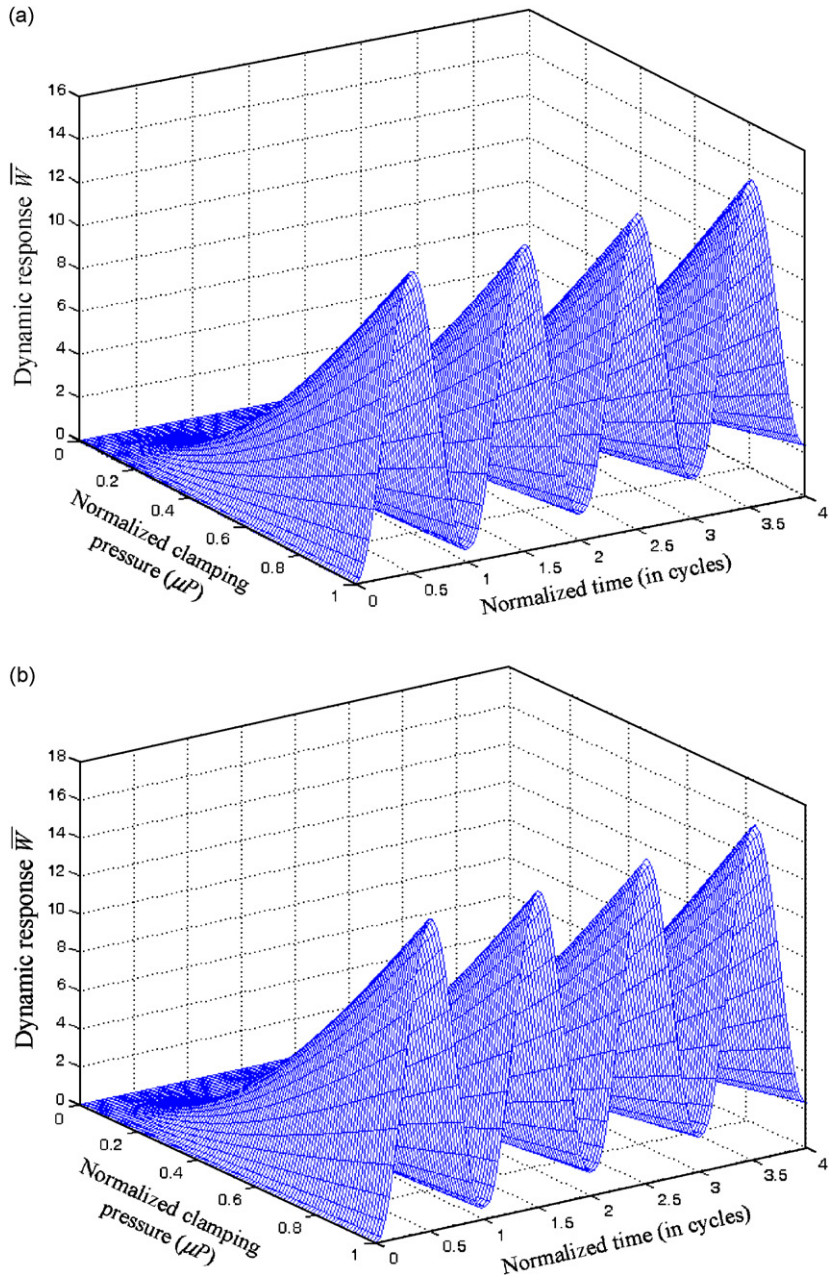

Fig. 5. Dynamic response profile to the forcing function $F = F_0 e^{i\omega t}$. (a) For the cases $\eta = 0.1$, $\varepsilon = 0$ and (b) $\eta = 0.1$, $\varepsilon = -0.2$.

6.1. Effects of frequency ratio on transverse displacement, slip and energy dissipation

The general picture of the dynamic response and slip at optimum interface pressure as illustrated in Figs. 7(a,b) and 9(a,b) respectively shows that the amplitude of vibration and the complementary interfacial slip increase with higher frequency ratio in the pre-resonance regime on the one hand and behave conversely post-resonance but based on the solution for static loading, we also expect our results to be strongly influenced by the nature of the pressure distribution along the interface. On the contrary, we find that the dominant role played by the pressure gradient in the ordering of the results for either the transverse response or slip is significantly subdued in the case of dynamic loading.

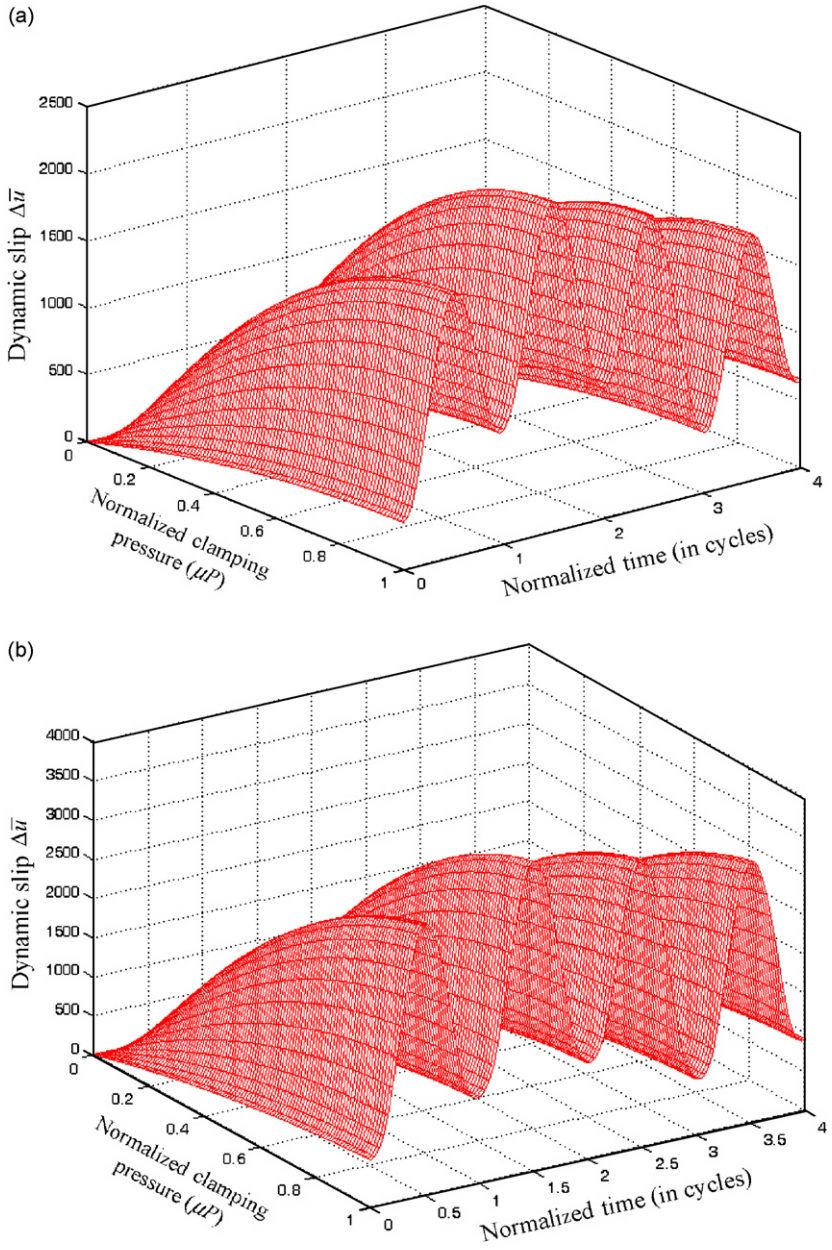

Fig. 6. Dynamic slip profile for the forcing function $F = F_0 e^{i\omega t}$. (a) For the cases $\eta = 0.5$, $\varepsilon = 0$ and (b) $\eta = 0.5$, $\varepsilon = -0.2$.

However, we also observe here that for any fixed frequency ratio η there is a departure from a uniform ordering and progression of either the beam response or the interfacial slip as a function of the pressure gradient ε with the highest values recorded for negative pressure gradient and the lowest for the most positive value of ε as was reported for the static problem. Instead, we observe, as shown in Figs. 8(b,c) and 10(a–c), respectively, that there is a tendency for the curves to bunch together without any clear cut ordering of the curves as a function of the pressure gradient ε. This does not apply to the same extent in the case of Fig. 8(a) where frequency ratio $\eta = 0.05$ is close to zero (Figs. 8–10).

The reason for this can be attributed to the cyclic nature of the optimal pressure. In this regard we may note that both the deflection and the interfacial slip at optimal pressure are necessarily functions of $\Delta(\eta)$ as

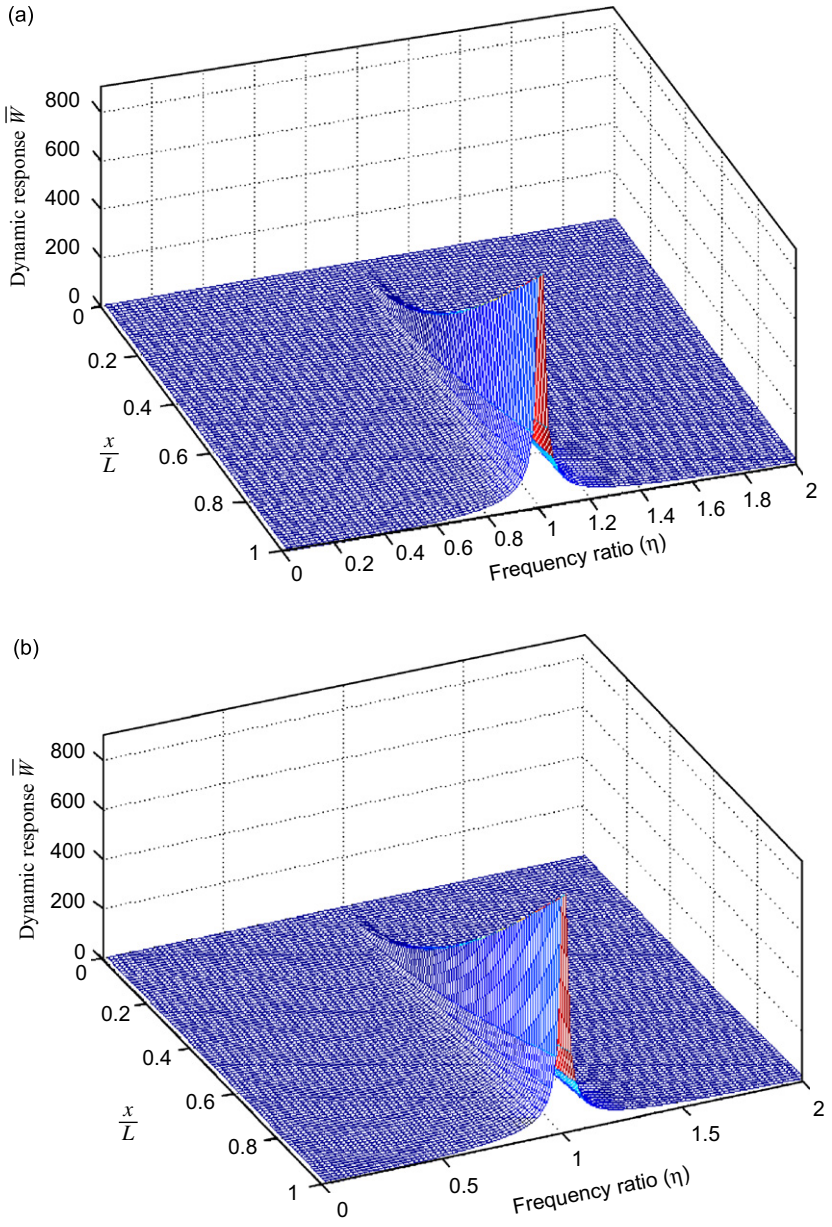

Fig. 7. Deflection at half cycle for optimum interface pressure (a) for the cases $\varepsilon = 0.2$ and (b) $\varepsilon = -0.2$.

established in Eq. (58a) and plotted in Fig. 11; this provides a mechanism for effective modulation or re-ordering of the deflection and slip profiles.

However, in the pre-resonance zone, the energy dissipation decreases with increase in the frequency ratio η as illustrated in Fig. 12. Nonetheless, this is not the full story because in the post-resonance zone, there are regions where the converse is true as illustrated in the energy spectrum displayed in Fig. 14. Furthermore, the bunching and relative re-ordering of curves at any fixed frequency ratio η observed above for the various values of the parameter ε in respect of the beam response and interfacial slip prevails in respect of the energy dissipation as shown in Fig. 13. The same observations can equally be made from a closer study of Fig. 14.

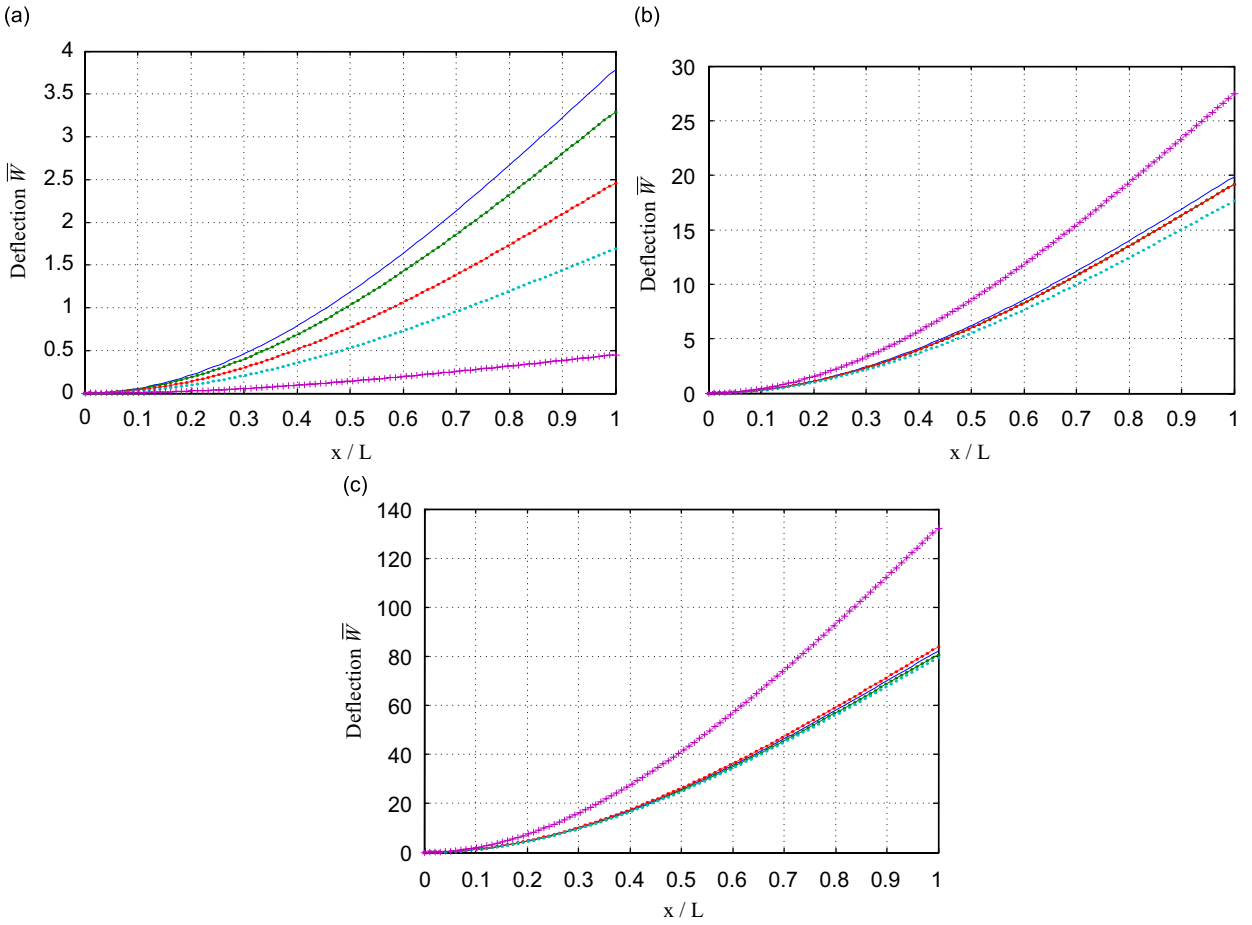

Fig. 8. Deflection at half cycle for optimum interface pressure (a) for the cases $\eta = 0.05$; (b) $\eta = 0.5$ and (c) $\eta = 0.85$. — $\varepsilon = 0$; $\varepsilon = 0.2$; ------ $\varepsilon = -0.2$; $\varepsilon = 0.6$; $\varepsilon = -0.6$.

6.2. *Effects of frequency ratio on logarithmic damping decrement and damping ratio*

With respect to the logarithmic damping decrement curve, we note that Nanda and Behera [27] did not specify the frequency range for their experiment. Nonetheless, the results reported by them when compared with our present results appear to be only part of the story. In fact, Nanda and Behera's results do not apply to cases where the frequency ratio η is very small, and their curves fail to capture the correct behaviour of δ for fairly small values of μP. This is clearly seen in Figs. 15(a–d). In particular, when we pick very small values for η and we restrict the normalized pressure to moderate values away from 0 (i.e. in the range $0.95 < \mu P < 10$), our graphs for the logarithmic damping δ are similar to those reported by Nanda and Behera (cf. Figs. 16(a–c). However, when we extend the range of μP closer to the origin, even for reasonably low values of η (e.g. $\eta = 0.05$), we find that the nature of the curve changes as shown in Fig. 15(a). Furthermore, for the extended range $0 < \mu P \leqslant 20$, we find that the curve for δ is in fact similar to that reported by Nishiwaki et al. in their 1978 and 1980 papers as reflected in Figs. 15(a–d).

In the past, it has been argued that in actual practice the interface pressure in press-fit joints or mechanical fasteners is never zero and plotting simulated curves for logarithmic damping decrement vs. μP starting from zero would therefore appear to be a mere theoretical exercise. However, this does not preclude the range $0 < \mu P \ll 1$ and the point to be made is that as long as the results for the logarithmic damping decrement obtained here is uniformly valid for various domains of μP as illustrated for example in Figs. 15(a–d). All previous results of earlier workers must be asymptotically recoverable from the present results as it was in

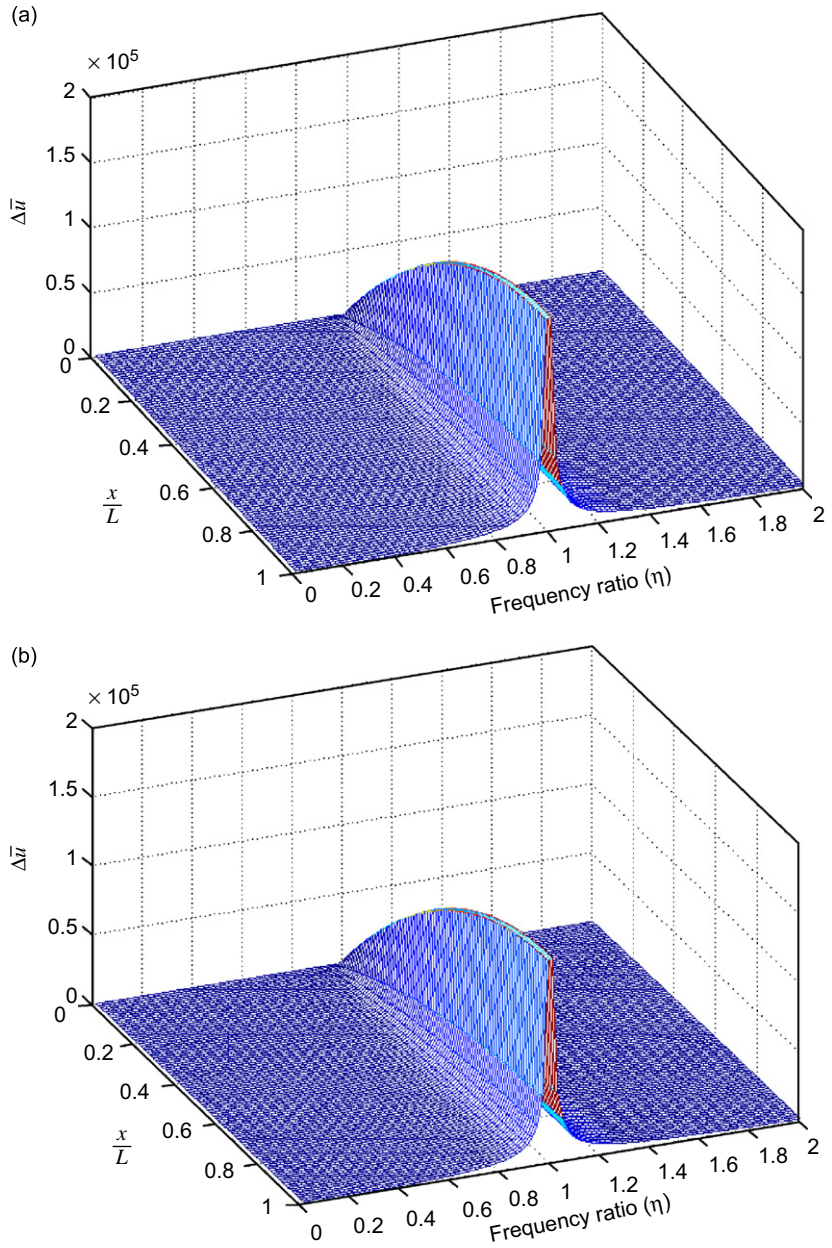

Fig. 9. Slip at half cycle for optimum interface pressure (a) for the cases $\varepsilon = 0.2$ and (b) $\varepsilon = -0.2$.

fact noted above that Nanda and Behera's plots for the logarithmic damping decrement did not cover small values of μP. It is in order to demonstrate that Nanda and Behera's results are embedded within those reported here that our figures have been blown up in different ranges of μP. Figs. 16(a–c) demonstrate that the Nanda and Behera plots can be recovered from the current solution if we restrict our attention like Nanda and Behera to the zone $1 < \mu P$; for example.

The general profile of logarithmic damping decrement curve clearly displays the existence of two regions that can be summarised as follows:

1. Starting from the origin and for very low values of pressure, δ is a monotonic increasing variable approaching a local peak. The peak value varies inversely as the frequency ratio η except in the

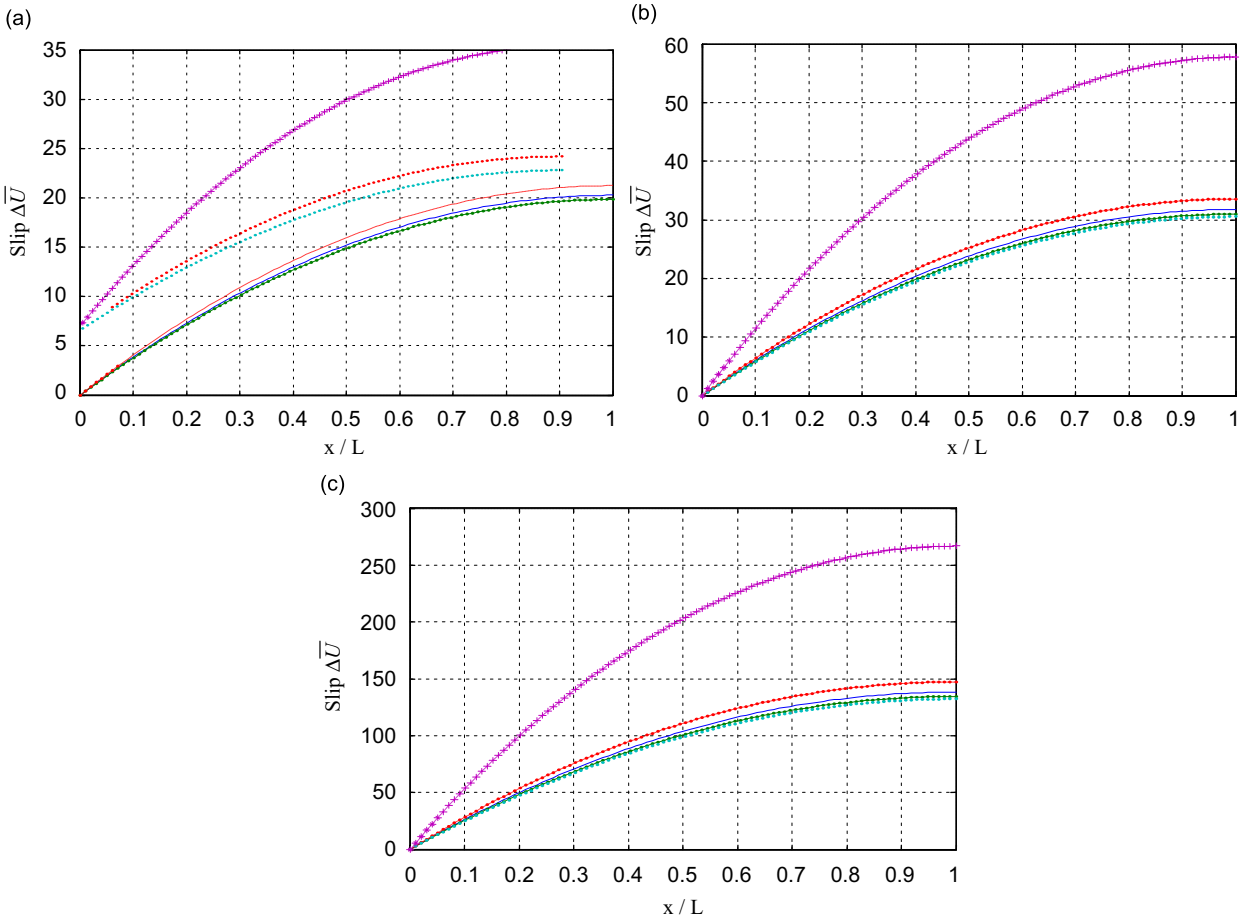

Fig. 10. Slip at half cycle for optimum interface pressure (a) for the cases $\eta = 0.30$; (b) $\eta = 0.5$ and (c) $\eta = 0.85$. — $\varepsilon = 0$; $\varepsilon = 0.2$; ------ $\varepsilon = -0.2$; $\varepsilon = 0.6$; $\varepsilon = -0.6$.

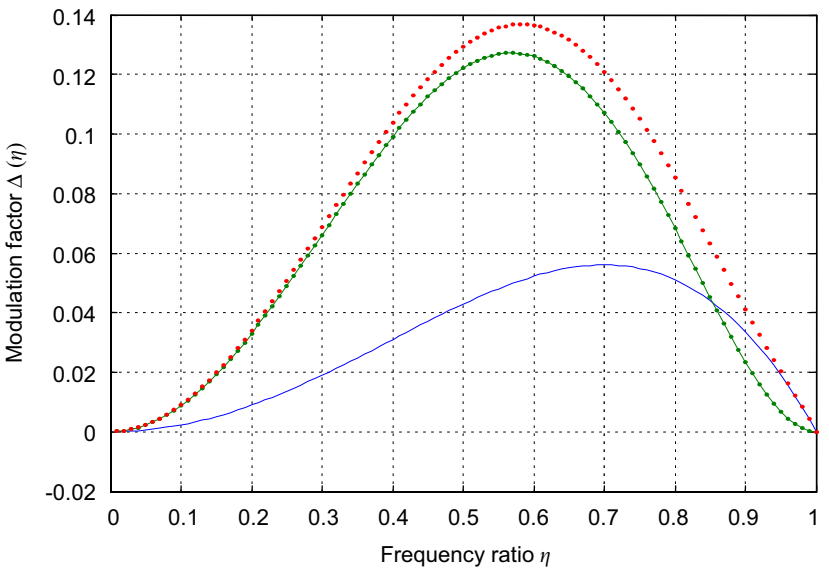

Fig. 11. Behaviour of frequency modulation factor as a function of η. — imaginary part; real part; ● modulus.

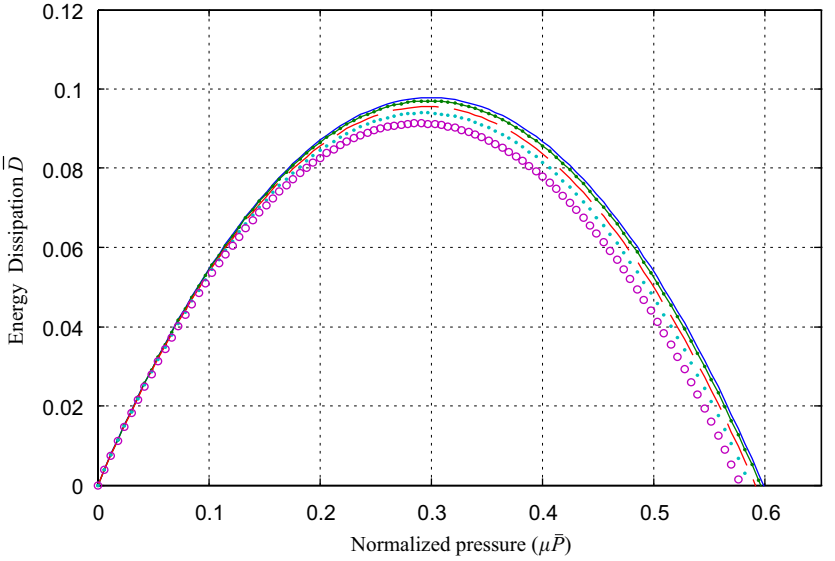

Fig. 12. Energy dissipation as a function of frequency ratio for $\varepsilon = -0.2$. — $\eta = 0.05$; $\eta = 0.30$; ------ $\eta = 0.05$; ● $\eta = 0.65$; ○ $\eta = 0.85$.

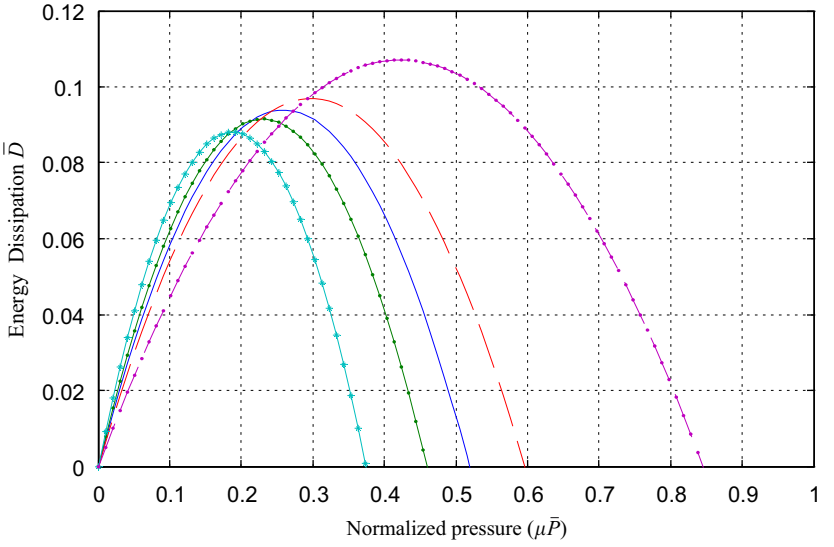

Fig. 13. Energy dissipation as a function of interfacial pressure gradient for $\eta = 0.3$. — $\varepsilon = 0$; $\varepsilon = 0.2$; ------ $\varepsilon = -0.2$; $\varepsilon = 0.6$; $\varepsilon = -0.6$.

neighbourhood of resonance. In this domain, the δ curves are ordered in consonance with the ε values. Thus δ curves for positive values of ε generally lie to the right of those with negative ε. We can call this region A.

2. The initial peak terminating region A is followed by a region B where the logarithmic damping decrement decreases monotonically to an asymptotic value characteristic of each case of η. As for a comparative analysis for different values of the interfacial pressure gradient ε, we find that the relative ordering of the δ curves for the different values of ε are in line with the ability to dissipate slip energy. Thus higher values of δ are recorded for cases when $\varepsilon < 0$. However, irrespective of the value of ε, the logarithmic damping decrement δ decreases as the value of μP increases reflecting a higher normal force at the interface of the laminates.

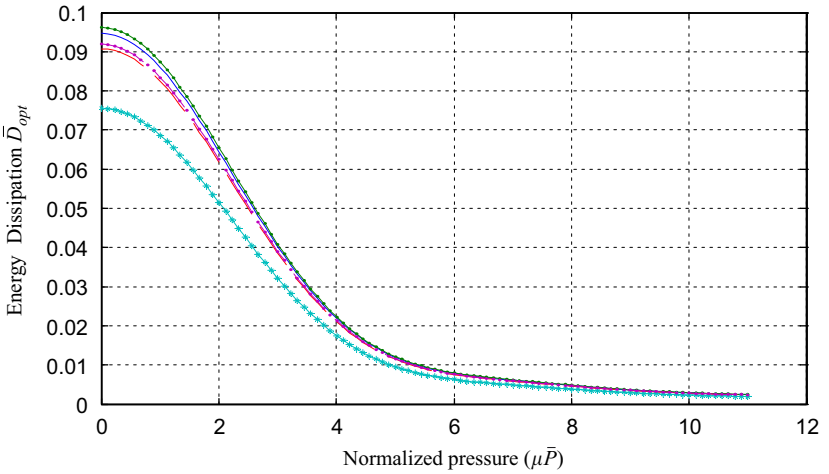

Fig. 14. Optimum energy dissipation as a function of frequency ratio η. — $\varepsilon = 0$; $\varepsilon = 0.2$; ------ $\varepsilon = -0.2$; $\varepsilon = 0.6$; $\varepsilon = -0.6$.

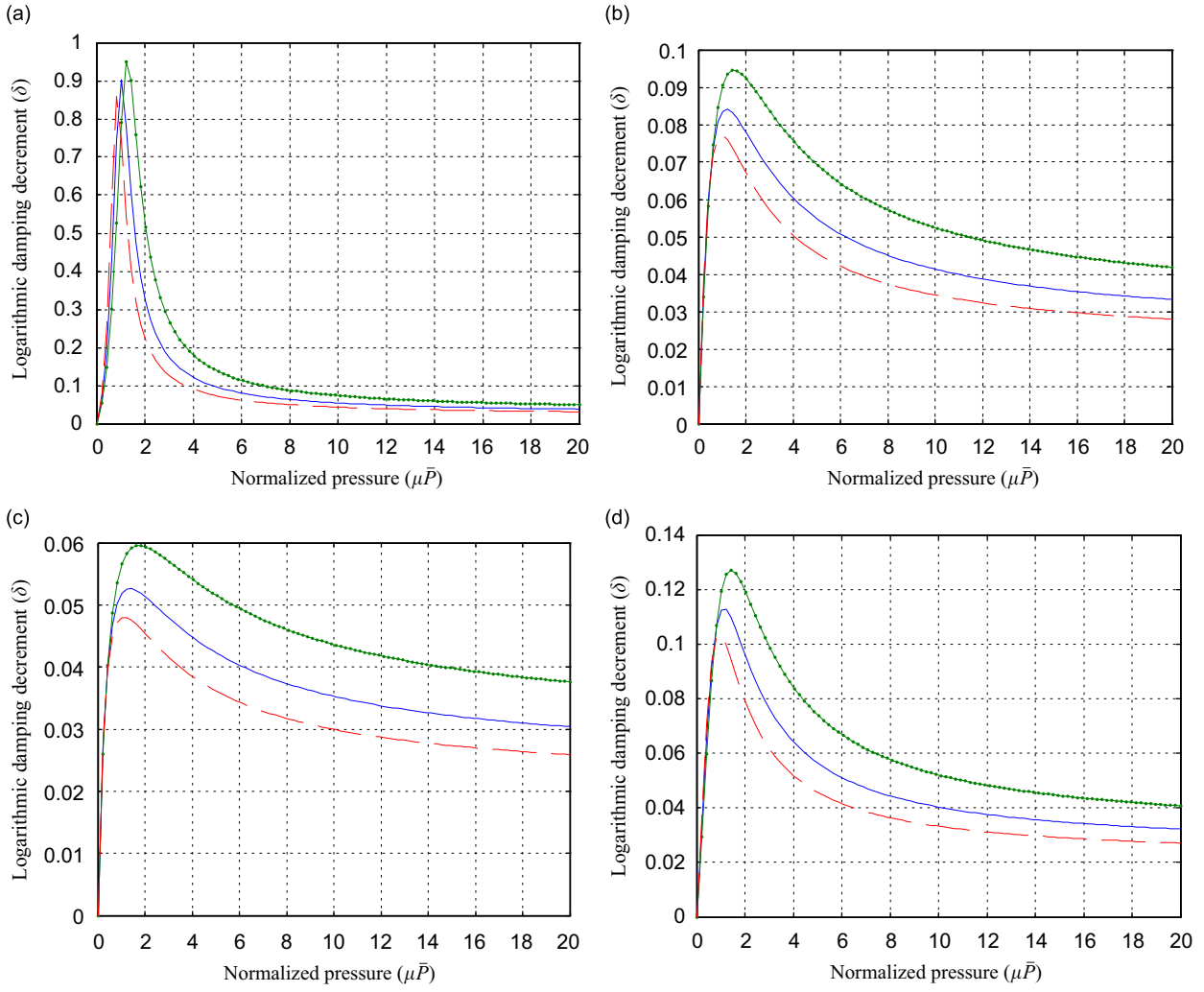

Fig. 15. Logarithmic damping decrement vs. interface pressure over entire pressure spectrum (a) for the cases $\eta = 0.05$; (b) $\eta = 0.3$; (c) $\eta = 0.5$ and (d) $\eta = 0.8$. — $\varepsilon = 0$; $\varepsilon = -0.2$; ------ $\varepsilon = 0.2$.

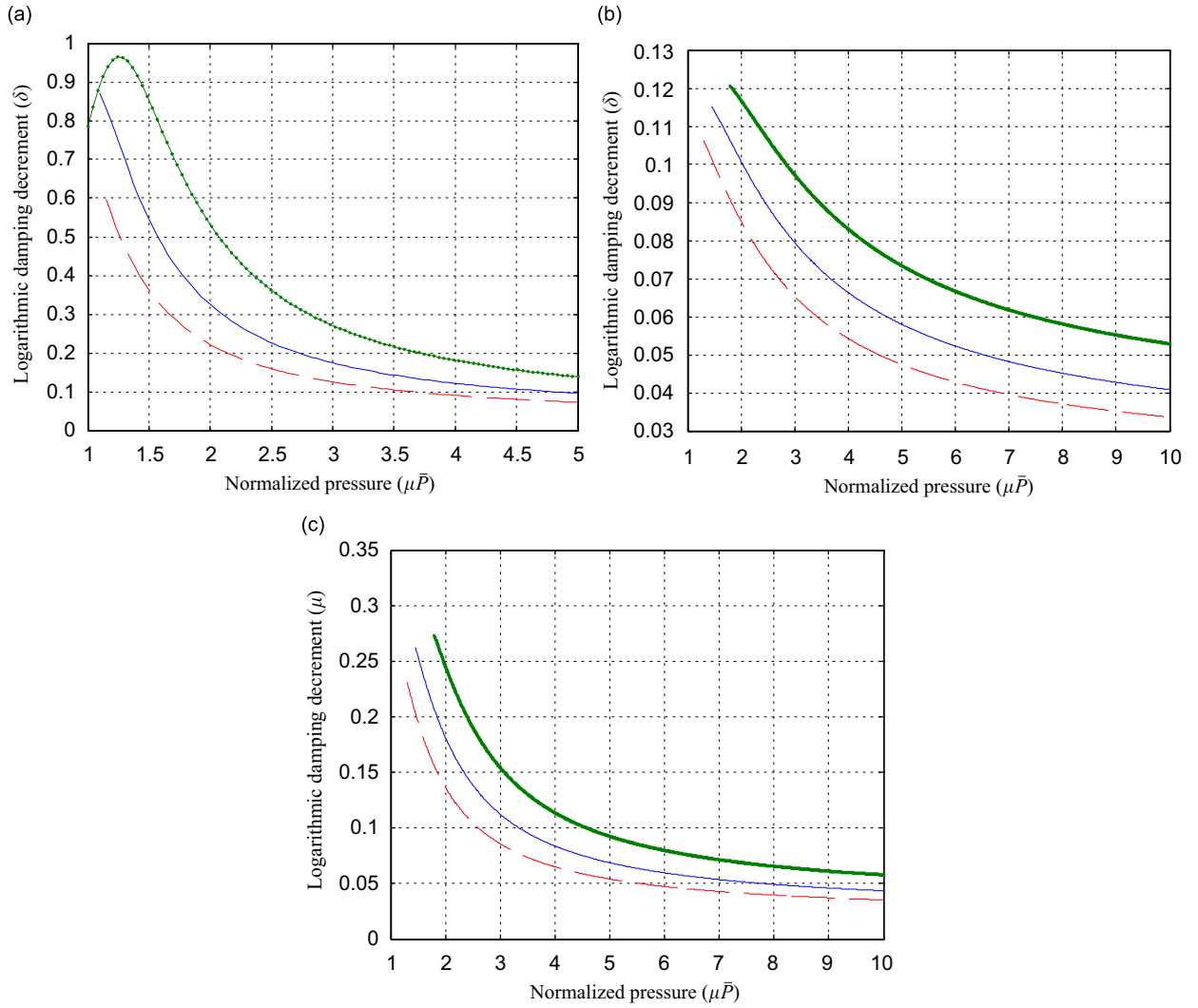

Fig. 16. Logarithmic damping decrement vs. interface pressure over restricted pressure spectrum (a) for the cases $\eta = 0.05$; (b) $\eta = 2$ and (c) $\eta = 3$. — $\varepsilon = 0$; -•- $\varepsilon = -0.2$; ------ $\varepsilon = 0.2$.

Having described the general profile, we must also recognise the fact that since the objective of our investigation is on the efficacy of slip damping, the entire curve for δ is of interest from the view point of engineering design and not just the behaviour within region B where δ curves are monotonically decreasing with increased pressure. It is therefore puzzling that Nanda and Behera limited their report to only zone B even though they conceded that they too found that "*the logarithmic damping decrement increases with an increase in the tightening torque in the lower range as established by Masuko et al. which is not viable in real application*". This statement appears curious as the general shape of the δ as derived in Eq. (57) must necessarily be driven by the shape of the slip energy equation which is shown to be parabolic in μP from Eq. (46a).

Three-dimensional plots for the logarithmic damping decrement δ and the damping ratio Ψ are plotted in Figs. 17 and 18 respectively as functions of the interfacial pressure and frequency ratio.

The corresponding results for the case of Heaviside forcing function need no special discussion as there are no new effects. However, all results for static loading can be fully recovered by restricting attention to the stationary component of the Heaviside forcing function solution.

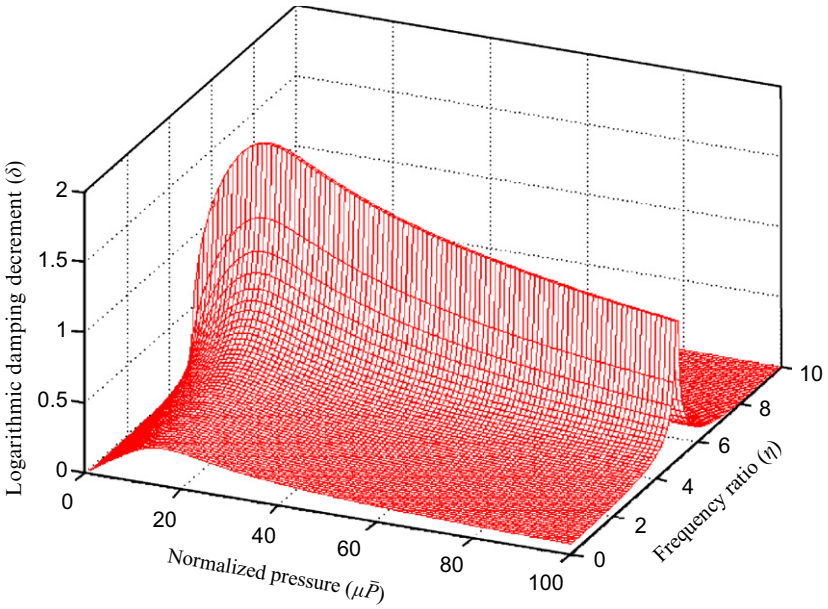

Fig. 17. Logarithmic damping decrement vs. interface pressure for $\varepsilon = -0.2$.

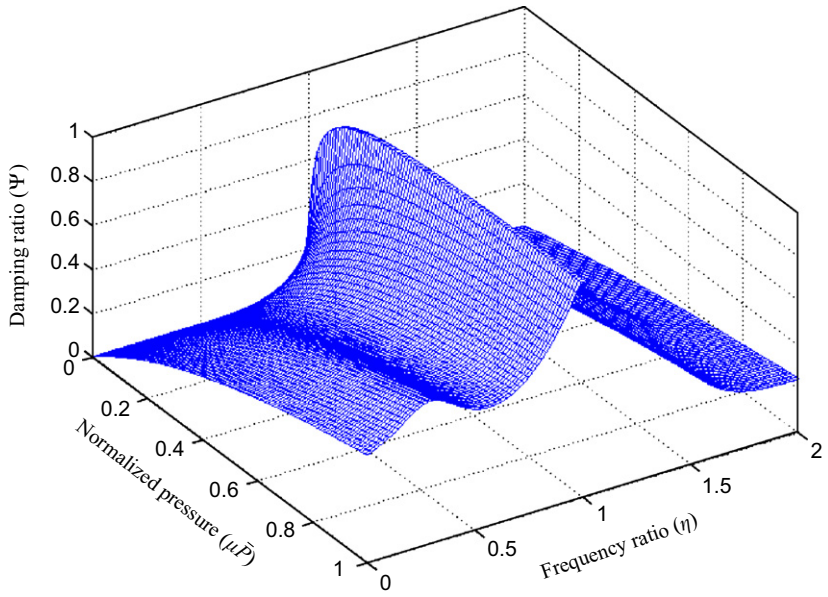

Fig. 18. Damping ratio vs. interface pressure and frequency ratio η for the case $\varepsilon = -0.2$.

7. Summary and conclusion

(a) In summary, we note that in this paper we have been able to find explicit solutions for the response, slip, optimal pressure and dissipated energy (i.e. W, Δu, P_{opt} and $\bar{D}$, respectively) for the layered cantibeam under both periodic and non-periodic forcing functions of the Heaviside type.

(b) While a lot of numerical, semi-analytic and experimental investigations abound in the literature for the layered cantibeam, this work is the first attempt to examine and present an analytical solution for the case of non-uniform interfacial pressure profile and shows that although results reported in the literature for

uniform pressure are correct, it is nonetheless possible to dissipate more energy than is predicted for the case of uniform interfacial pressure profile. The required condition for this is that: $dP_{av}/dx<0$. One way of simulating such a pressure distribution is by progressively reducing the tightening torque on the bolts holding the laminates as one moves from the clamped to the free end of the cantibeam. This can be the subject of further experimental work. It is also conceivable that following the work of Nanda and Behera, different interface pressure distribution patterns can be simulated by varying parameters such as number and size of bolts, number of laminated layers and washers, etc.

(c) Having made the above observation, the next thing to note here is that the amount of energy that can be dissipated through slip damping under externally applied dynamic load is less than the corresponding value for the static case. This is not a new result as the same point was made by Goodman and Klumpp [1] several decades ago; however, what is of interest here is to see how the amount of slip energy that can be generated is influenced by factors like the interfacial pressure distribution on the one hand and the frequency ratio on the other.

(d) The frequency ratio η has its modulating effect on the various outputs of our problem. For example in the pre-resonance zone, increasing frequency ratio η has the effect of enhancing both the transverse displacement and interfacial slip. Outside the resonance zone, the converse however holds in the case of dissipated energy through slip. We also note from Eq. (58a) in respect to P_{opt} that the effect of η is to modulate the value of μP_{opt} since curve for $\Delta(\eta)<1$ for all values of η as shown in Fig. 11.
This then means that the maximum energy that can be dissipated through slip occurs at a lower optimal pressure and is less than what is obtained in the static case. Thus, in this respect, the effect of a forcing function is to simultaneously lower the required externally applied interface pressure while reducing the amount of energy dissipation. In practical terms and for the case of layered and jointed sections such a reduction in the externally applied interfacial pressure could translate to the use of less number of bolts and washers or an increase in the spacing in between such bolts. Alternatively, it may also lead to a reduction in the sizes of such bolts as compared to what would be needed for the case of external static load.

(e) With respect to the logarithmic damping decrement, the first thing to note here is that the derivation of the expression for the logarithmic damping decrement is based on a formulation that is different from that used by previous workers (i.e. Masuko, Nanda, Behera, etc.). Thus there is a need for comparison of our results with those of earlier workers. Secondly, the results for the logarithmic damping as obtained by earlier workers were either graphical or limited to different ranges of μP. In particular, Masuko's results were limited to small values of μP whilst those of Nanda and Behera prevail outside this range. However, the analytical result presented for the logarithmic damping decrement in this work is uniformly valid in the various domains of μP and being more generalised, is not constrained by the assumption implicit in the Maclaurin series expansion adopted by earlier workers. As a check, it is shown that the reported results agree with the work of Masuko on the one hand for $\mu P \ll 1$ and that of Nanda and Behera outside this range.
On the issue of comparison of results, we find that for small values of μP, for which Nanda and Behera did not present any results, there is close agreement between our results and those reported earlier by Masuko et al. [4]. On the other hand, outside this domain, the results of Nanda and Behera [23] can also be recovered from our generalised results.
The good agreement between the two results is quite reassuring in that whereas the solutions in Nanda and Behera are couched in the context of bolt sizes, their location and number, the present result depends more on the average interface pressure and its gradient. This is however not surprising as the work of Nanda and Behera has shown that the effect of the bolts, washers, their sizes and locations is to determine the pattern of the pressure distribution along the laminate interface.

(f) On the combined effect of pressure gradient and frequency ratio η, our results do not show any clear pattern that the combined effects of these factors are directly cumulative especially as they moderate the displacement and slip. This aspect of the work would need further investigation.

These results can be positively exploited in the design of aerodynamic and machine structures. They can also be extended to vibrating plates and shells of different materials and dimensions.

References

[1] L.E. Goodman, J.H. Klumpp, Analysis of slip damping with reference to turbine blade vibration, *Journal of Applied Mechanics* 23 (1956) 421.

[2] C. Cockerham, G.R. Symmons, Stability criterion for stick-slip motion using a discontinuous dynamic friction model, *Wear* 40 (1976) 113–120.

[3] D.P. Hess, et al., Normal vibrations and friction at a Hertzian contact under random excitation: theory and experiment, *Journal of Sound and Vibration* 153 (3) (1992) 491–508.

[4] A. Guran, et al., *Dynamic with Friction. Modeling, Analysis and experiment, Series on Stability, Vibration and Control of Systems*, World Scientific, Singapore, 1996.

[5] D.M. Barnett, et al., Slip wave along the interface between two anisotropic elastic half-space in sliding contact, *Proceedings of the Royal Society of London, Series A* 415 (1988) 389–419.

[6] G.A. Maugin, et al., Interfacial waves in the presence of areas of slip, *Geophysical Journal International* 118 (1994) 305–316.

[7] M. Gosz, et al., Effect of viscoelastic interface on the transverse behavior of fiber-reinforced composites, *International Journal of Solid and Structures* 27 (1991) 1757–1771.

[8] M. Masuko, Y. Ito, K. Yoshida, Theoretical analysis for a damping ratio of jointed cantibeam, *Bulletin of JSME* 16 (1973) 1421–1432.

[9] N. Nishiwaki, M. Masuko, Y. Ito, I. Okumura, A study on damping capacity of a jointed cantilever beam (1st Report; experimental results), *Bulletin of JSME* 21 (1978) 524–531.

[10] N. Nishiwaki, M. Masuko, Y. Ito, I. Okumura, A study on damping capacity of a jointed cantilever beam (2nd Report; comparison between theoretical and experimental results), *Bulletin of JSME* 23 (1980) 469–475.

[11] M. Motosh, Stress distribution in Joints of bolted or riveted connections, *Transactions of ASME, Journal of Engineering for Industry* (1975).

[12] I. Ferlund, *Method to Calculate the Pressure Between Bolted or Riveted Plates*, Transactions of Chalmers University of Technology, Gothenberg, Sweden, 1961, p. 245.

[13] T.J. Lardner, Stress analysis for thermal contact resistance across bolted joints, *Transactions of ASME, Journal of Applied Mechanics* 32 (1965) 458–459.

[14] O.T. Sidorov, Change of the damping of vibrations in the course of operation in dependence on the parameters of bolted joints, *Strength of Materials* 14 (1983) 671–674.

[15] R.M. El-Zahry, Investigation of the vibration behaviour of pre-loaded bolted joints, *Dirasat-Engineering Technology* 12 (1985) 201–223.

[16] T. Kaboyashi, T. Matsubayashi, Consideration on the improvement of the stiffness of bolted joints in machine tools, *Transaction of the Japan Society of Mechanical Engineering* 52 (1986) 1092–1096.

[17] T. Kaboyashi, T. Matsubayashi, Consideration on the improvement of the stiffness of bolted joints in machine tools, *Bulletin of JSME* 29 (1986) 3934–3937.

[18] J.S. Tsai, Y.F. Chou, Modelling of dynamic characteristics of two-bolted joints, *Journal of Chinese Institute of Engineering* 11 (1988) 235–245.

[19] Y.S. Shin, J.C. Iverson, K.S. Kim, Experimental studies on damping characteristics of bolted joints for plates and shells, *Trans ASME, Journal of Pressure Vessel Technology* 113 (1991) 402–408.

[20] S. Song, C. Park; K.P. Moran, S. Lee, Contact area of bolted joints interface; analytical, finite element modelling and experimental study, *ASME, EEP* 3 (1992) 73–81.

[21] H.H. Gould, B.B. Mikic, Areas of contact and pressure distribution in bolted joints, *Transactions of ASME, Journal of Engineering for Industry* (1972) 864–870.

[22] H.H. Ziada, A.K. Abd, Load pressure distribution and contact areas in bolted joints, *Institute of Engineers (India)* 61 (1980) 93–100.

[23] B.K. Nanda, A.K. Behera, Damping in layered and jointed structures, *International Journal of Acoustics and Vibration* 5 (2) (2000) 89–95.

[24] B.K. Nanda, A.K. Behera, Improvement of damping capacity of structured members using layered construction, in: Seventh International Congress on Sound and Vibration, Garmisch-Partenkirchen, Germany, 2000, pp. 3059–3066.

[25] S.W. Hansen, R. Spies, Structural damping in laminated beams due to interfacial slip, *Journal of Sound and Vibration* 204 (1997) 183–202.

[26] B.K. Nanda, Study of damping in structural members under controlled dynamic slip, Ph.D. Thesis, Sambalpur University, 1992.

[27] B.K. Nanda, A.K. Behera, Study on damping in layered and jointed structures with uniform pressure distribution at the interfaces, *Journal of Sound and Vibration* 226 (4) (1999) 607–624.

[28] B.K. Nanda, Study of the effect of bolt diameter and washer on damping in layered and jointed structures, *Journal of Sound and Vibration* 290 (2006) 1290–1314.

[29] O. Damisa, V.O.S. Olunloyo, C.A. Osheku, A.A. Oyediran, Static analysis of slip damping with clamped laminated beams, *European Journal of Scientific Research*, 17 (4) (2007) 455–476, ISSN 1450-216X.

[30] V.O.S. Olunloyo, O. Damisa, C.A. Osheku, A.A. Oyediran, Further results on static analysis of slip damping with clamped laminated beams, *European Journal of Scientific Research*, 17 (4) (2007) 491–508, ISSN 1450-216X.

[31] C.A. Osheku, Application of beam theory to machine, aero and hydro-dynamic structures in pressurized environments, Ph.D. Thesis, University of Lagos, Nigeria, 2005.

[32] O. Damisa, Slip damping of Timoshenko beam close to resonance, *JER* 11 (1 and 2) (2003) 13–26.